1974

Laser holographic interferometric investigation of heat transfer about an isothermal vertical flat plate

Richard Michael Quinlisk

Department:

LASER HOLOGRAPHIC INTERFEROMETRIC INVESTIGATION OF HEAT TRANSFER ABOUT AN ISOTHERMAL VERTICAL FLAT PLATE

BY

RICHARD MICHAEL QUINLISK, 1949 -

A THESIS

Presented to the Faculty of the Graduate School of the

UNIVERSITY OF MISSOURI-ROLLA

In Partial Fulfillment of the Requirements for the Degree

MASTER OF SCIENCE IN MECHANICAL ENGINEERING

1974

Approved by

R J Reilly (Advisor)

ABSTRACT

A study of the laser holographic interferometer was conducted to compare heat transfer data obtained with the device to standard free convection boundary layer theory. The system studied was an isothermal vertical flat plate. The interferometer was used to obtain fringe patterns of the boundary layer at the plate surface.

Data from the holographic interferograms were recorded by making conventional two-dimensional photographs of the holographic images.

The optical data are shown to have a good correlation to Von-Karman theory. Values of the boundary layer thickness, temperature distribution, and heat transfer were compared. An attempt was made to probe the boundary layer with a conventional thermocouple in an effort to provide a third type of comparative data.

The laser holographic interferometer was shown to be an excellent instrument for obtaining quantitative heat transfer measurements in the gaseous boundary layer.

ACKNOWLEDGEMENTS

The author is deeply grateful to Dr. R. L. Reisbig for his guidance and insight throughout the course of this experiment. The author also wishes to acknowledge Dr. L. G. Rhea and Dr. Tsoulfanidis for their patience over the period of this endeavor.

In addition, the author acknowledges Jill McCartney for her assistance in typing the rough draft and Mary Quinlisk, who patiently waded through the final draft of this thesis.

Finally, appreciation is extended to the Mechanical Engineering Department for the teaching assistantship which made this work financially possible.

TABLE OF CONTENTS

	Page
ABSTRACT	ii
ACKNOWLEDGEMENTS	iii
TABLE OF CONTENTS	iv
LIST OF ILLUSTRATIONS	v
LIST OF TABLES	vi
LIST OF SYMBOLS	vii
I. INTRODUCTION	1
II. LASER HOLOGRAPHIC INTERFEROMETRY PROCESSES	3
A. Laser Holographic Interferometry	3
B. Boundary Layer Model	4
C. Optical Theory	8
III. EXPERIMENTAL APPARATUS	13
A. The Table	13
B. The Laser and Optical Components	13
C. The Test Section	15
IV. TEST PROCEDURE	21
V. RESULTS	24
VI. CONCLUSIONS	45
BIBLIOGRAPHY	46
VITA	48
APPENDICES	49
I. ERROR ANALYSIS	50
II. THERMOCOUPLE CONSTRUCTION AND CALIBRATION	54

LIST OF ILLUSTRATIONS

Figure		Page
1	Boundary Layer form an Isothemal Vertical Flat Plate	6
2	System Apparatus.	14
3	Nichrome Wire Layout and Thermocouple Locations	16
4	Thermocouple Installation Detail.	18
5	Test Plate and Mount.	19
6	Schematic of Apparatus.	22
7	Interferograms of First 100°F Plate	25
8	Interferograms of Second 100°F Plate.	26
9	Interferograms of 125°F Plate	27
10	Close-up of Figure 9b	28
11	Boundary Layer Thickness for Air (Exp. 1) . . .	32
12	Boundary Layer Thickness for Air (Exp. 2) . . .	33
13	Boundary Layer Thickness for Air (Exp. 3) . . .	34
14	Air Temperature Profile in Boundary Layer (Exp. 1).	36
15	Air Temperature Profile in Boundary Layer (Exp. 2).	37
16	Air Temperature Profile in Boundary Layer (Exp. 3).	38
17	Heat Transfer Data (Exp. 1)	40
18	Heat Transfer Data (Exp. 2)	41
19	Heat Transfer Data (Exp. 3)	42
20	Number of Fringes	44
21	Thermocouple Calibration Curve.	55

LIST OF TABLES

Table		Page
I.	Thermocouple Data for First 100°F Plate	29
II.	Thermocouple Data for Second 100°F Plate.	30
III.	Thermocouple Data for 125°F Plate	31
IV.	Data for Error Analysis	52

LIST OF SYMBOLS

A	Test plate area, in^2
dL	Estimated error in plate length, in
$dT_{p.t.}$	Estimated error in temperature due to plate surface variations, °F
$dT_{t.c.}$	Estimated error in thermocouples, °F
Gr_x	Grashof number, $g\beta \frac{(T_w - T_\infty)}{\nu^2} x^3$
g	Acceleration due to gravity, ft/sec^2
H	Plate height, in
K	Gladstone-Dale constant, $\frac{ft^3}{lb_m}$
L	Test plate length, in
L_+	Theoretical test plate length, in
m	Number of fringes
n	Index of refraction
P	Pressure, psi
Pr	Prandtl number, $\frac{\nu}{\alpha}$
q	Heat transfer BTU/hr
R	Universal gas constant $ft\text{-}lb_f/lb_m\text{-}^\circ R$
F	Specific refraction, ft^3/lb_m
T	Temperature, °F
T_i	Known temperature in fringe system, °F
T_{m+i}	Temperature in fringes from known temperature, °F
T_∞	Ambient air temperature, °F
T_w	Plate wall temperature, °F
u	Velocity in x-direction, ft/sec

x	Coordinate along test plate, ft
y	Coordinate normal to test plate, ft.

GREEK SYMBOLS

α	Thermal diffusivity, ft/hr-°F
β	Coefficient of thermal expansion, 1/°F
δ	Boundary layer thickness, in
κ	Thermal conductivity, BTU/hr-ft^2-°F
λ_o	Wavelength of light in a vacuum, Å
υ	Kinematic viscosity, ft^2/sec
ρ	Density, lb_m/ft^3

I. INTRODUCTION

Accurate temperature measurement has been the subject of study for some time. The most widely used instruments have been various thermometers and thermocouples. Because of thermophysical properties of the materials used, these instruments cannot be used in extremely high temperature regions.

More recently, optical interferometry has been used to make measurements of temperature fields. Optical methods do not suffer from the above-mentioned limitations. The major portion of the work in the field has been conducted using the Mach-Zehnder interferometer. Despite the high quality fringe patterns obtained, the system has distinct disadvantages. These are discussed in detail by Thomson [1]*.

The latest application of optical methods has been the laser holographic interferometer. A recent study was conducted by Thomson [1]. His thesis laid the groundwork for a further study reported in a thesis by Reifel [2]. These two theses illustrated the usefulness and application of laser holographic interferometry to heat transfer studies.

Another recent paper, by A. E. Zinnes [3], used the laser holographic interferometer to obtain experimental corroboration with numerical methods used to model free convection boundary layers along plates with arbitrary temperature distributions.

---

*Bracketed numbers indicate references cited in Bibliography.

Because of the relatively low cost and ease of operation, laser holography will gain wider use in the field of optical interferometry applied to heat transfer data in the near future. A rather complete discussion of potential applications to heat transfer studies of interferometry is presented by Hauf and Grigull [4].

This study was initiated to establish the utility of the laser holographic interferometer as a device to measure heat transfer. A simple-two-dimensional free convection boundary layer in the neighborhood of an isothermal vertical flat plate was obtained. Procedurally, there is no difference in this study or those conducted by Thomson or Reifel. The difference is in the system observed. Thomson simply heated his apparatus at the bottom to create a varying plate temperature. Reifel's system is simultaneously heated and cooled to create a linear plate temperature distribution at the surface. Von-Karman-type integral solutions [5] were compared to the data from the interferometer used in this study.

II. LASER HOLOGRAPHIC INTERFEROMETRY PROCESSES

A. Laser Holographic Interferometry

In order that the reader understand the basic principles and operation of the laser holographic interferometer, a brief background will be given and the methods used to make a hologram will be discussed.

The introduction of holography came about in 1948 during which time there was a great, but short-lived, flurry of activity. This activity experienced a rebirth on a large scale during 1962. In that time, there were a great number of proposed uses, one of which was interferometry.

Two studies were conducted in the mid-1960's. The first, entitled "Holographic Interferometry" [5], was an excellent qualitative study of interferometry. Many illustrations were given and complete descriptions of optical systems were described, but there was no attempt to make any quantitative deductions at that time. A second paper, "New Dimensions for Interferometry," by R. E. Brooks [6] followed the same theme as the previous work with new illustrations but, again there was no quantitative results included.

There are four basic types of holographic interferometers used. They are designated single-exposure, double-exposure, time-average, and contour generation. A detailed discussion of these four methods can be found for the reader's information, in a book by Smith [7].

The type used in this study was the double-exposure holographic interferometer. A laser was used to provide a monochromatic and highly coherent light source, which is necessary for good results. The light beam was split into two beams, an object beam, directed through the disturbed region, and a reference beam, directed at the holographic plate. It is this object beam that experiences path deviations due to changes in the refractive index of the air before reaching the recording medium. Since both object and reference beams are mutually coherent, they create an interference pattern in the form of a fringe system. This complex system is microscopic in nature, owing its unique detail to the object beam. In the method used, the first exposure was made of the system in its ambient state. The second exposure was made after the system had reached the disturbed state to be studied. During the interim period, no movement of the plate or system was allowed. This procedure caused a superimposition in the photographic emulsion of the plates, recording any changes in the system between each exposure. When illuminated by a beam of light of the same wavelength, reconstruction of the object beam occurs during the fringe system caused by the disturbance. The design of a similar system was described in a paper by Reisbig [8].

B. Boundary Layer Model

As was stated in the introduction, this experiment has

the purpose of establishing the capability of the laser holographic interferometry to heat transfer measurements. This implies the necessity of comparing results obtained with the interferometer with accepted theory.

For a theoretical analysis of this problem, a detailed study is presented in Holman [9]. A condensed version will appear in this thesis. Figure 1 will serve as visual aid for this analysis. The boundary layer is two dimensional and the gas has constant properties. The x-axis is established along the surface of the vertical plate and the y-coordinate is perpendicular to the plate. The equation used in the analysis is the integral energy equation for laminar flow.

$$\frac{d}{dx}\left[\int_0^\infty u\,(T - T_\infty)\right] = -\alpha \left.\frac{\partial T}{\partial y}\right|_{y=0} \qquad (1)$$

The boundary conditions governing the solution of this problem are:

$T = T_\infty$ at $x = 0$

$T = T_w$ at $y = 0$

$T = T_\infty$ at $y = \delta$

$\frac{dT}{dy} = 0$ at $y = \delta$

With the application of these conditions, integration of the energy equation yields the following temperature distribution,

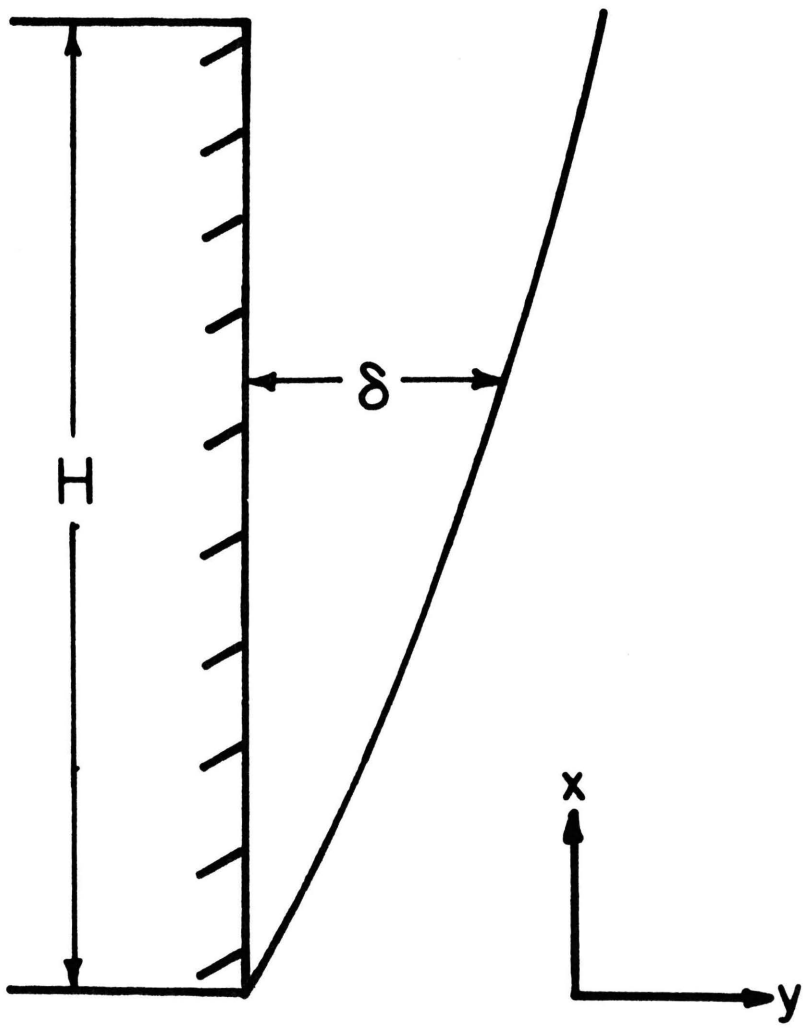

FIG. 1 BOUNDARY LAYER FROM AN ISOTHERMAL VERTICAL FLAT PLATE

$$\frac{T - T_\infty}{T_w - T_\infty} = (1 - \frac{y}{\delta})^2 \qquad (2)$$

Equation (2) now gives a theoretical basis for comparison of the data obtained with holographic methods. But it is still necessary to obtain an equation for the boundary layer thickness.

To accomplish this, the integral momentum equation is employed

$$\int_o^\delta \frac{\delta u^2}{\delta x}\, dy - g\beta \int_o^\delta (T - T_\infty)\, dy - \frac{\partial u}{\partial y}\Big|_{y=0} \qquad (3)$$

The boundary conditions are as follows:

$u = 0$ at $x = 0$

$u = 0$ at $y = 0$

$u = 0$ at $y = \delta$

$\frac{\partial u}{\partial y} = 0$ at $y = \delta$

When the equation for the velocity distribution is assumed to be a cubic, then through the use of these boundary conditions and careful manipulation, integration of equation (3) yields

$$\frac{\delta}{x} = 3.93\ Pr^{-1/2}\ (.952 + Pr)^{1/4}\ Gr_x^{-1/4} \qquad (4)$$

The Grashof number, Gr_x, is a function of x^3 which makes δ a function of $x^{1/4}$.

Now that relationships for the temperature distribution and boundary layer thickness have been found, they can be introduced to

$$\frac{q}{A} = -\kappa \left.\frac{\partial T}{\partial y}\right|_{y=0} \tag{5a}$$

which is the boundary condition for heat transfer from the vertical flat plate to obtain

$$\left(\frac{q}{A}\right)_{wall} = \kappa\,(T_w - T_\infty) \cdot 2/\delta \tag{5b}$$

Equation (5b) is the final form of the heat transfer equation which will be used for comparative analysis with the results obtained from the interferometer.

C. Optical Theory

In 1880, Lorenz and Lorentz deduced a theoretical formula for the relationship of density and the index of refraction.

This relationship

$$\frac{n^2-1}{n^2+2} \cdot \frac{1}{\rho} = \text{const.} \tag{6}$$

was later reconfirmed with a different theory by Planck. This theory was shown to be practical for many substances from gaseous to liquid states over wide variations in pressure and temperature [10].

As shown in Langhurst [10], equation (6) may be

rewritten as

$$\frac{n-1}{\rho} \cdot \frac{n+1}{n^2+2} = \text{const.}$$

> "Now for a gas, the refractive index does not differ widely from unity, so that the second factor is almost constant. Hence for a gas, one has
>
> $$\frac{n-1}{\rho} = \text{const.} \qquad (7)$$
>
> which is the law of Gladstone-Dale." [10]

The Gladstone-Dale law is then a special case of the Lorenz-Lorentz equation for a perfect gas.

The Lorenz-Lorentz equation has also been referred to as the "specific refraction." This value is expressed as $\bar{r}$, and is discussed further by Hauf and Grigull [4]. When related to the Gladstone-Dale equation, Hauf and Grigull write what they refer to as the "amplified" form of the Lorenz-Lorentz equation for a value of n near unity

$$\frac{2\,(n-1)}{3\rho} = \bar{r} = \text{const.} \qquad (8)$$

Substitution of equation (8) into equation (7) yields

$$K = 3/2\ \bar{r} = \text{const}$$

for gases.

Since work on this experiment was conducted with the gas in moderate temperature regions, one may employ the equation of state for an ideal gas to relate the

Gladstone-Dale equation to temperature changes rather than changes in density. Therefore,

$$P = \rho RT \tag{9}$$

For a constant pressure system

$$(\Delta T) = - \frac{RT^2}{P} (\Delta \rho) \tag{10}$$

By relating this to the finite difference form of equation (7), small temperature changes may be related to small changes in refractive index,

$$(\Delta T) = - \frac{RT}{KP} (\Delta n) \tag{11}$$

The use of equation (11) has been explained by Reifel [2]. Reifel conducted a mathematical analysis of the monochromatic light rays passing through a gaseous medium. This analysis took into account both the effects due to deflection and phase shift. Due to phase shift, successive fringe shifts will appear ". . .when the relative phase shifts at the photographic plate are exact multiples of 2π. . ." [2]. This requires all fringe shift measurements to cover the distance from the beginning of one bright area to the next bright area.

Reifel's results showed that density variation may be written as

$$\frac{2\pi LK}{\lambda o} (\rho_b - \rho_a) - 2\pi m, \quad m=0, 1, 2, 3, \ldots \tag{12}$$

or

$$\Delta\rho = \frac{m\lambda o}{LK} \tag{13a}$$

where m is the number of fringes covered in the analysis. Furthermore, this gives the value of density change between two adjacent fringes as a constant value

$$\Delta\rho = \frac{\lambda o}{LK} \tag{13b}$$

Coupling equations (10) and (13b) yields an expression for the temperature change between two adjacent fringes dependent merely on a set of fixed parameters,

$$\Delta T = \frac{\lambda o R T_i^2}{KLP} \tag{14a}$$

where T_i is a known temperature in the fringe system. Reifel further expanded his results to account for temperature changes over any set of fringes, which is given by

$$T_{m+i} - T_i = \frac{m\lambda o R T_i^2}{LKP} \quad . \tag{14b}$$

As a means of comparison of the visual results of the holograms to the Gladstone-Dale predictions, equation (14b) may be rewritten to solve for the number of fringes predicted by this theory. This equation gives the number of fringes as

$$m = \frac{LKP}{\lambda o R}\left(\frac{T_{m+i} - T_i}{T_i^2}\right) \tag{15}$$

Equation (12) leads to the observation that each fringe is a line of constant density, and the equation of state of an ideal gas further implies that each fringe is a line of

is a line of constant density, and the equation of state of an ideal gas further implies that each fringe is a line of constant temperature, if pressure is not varied.

With the above considerations, an equation for the heat transfer based on the Gladstone-Dale law can be found. The heat transfer at a plate surface is given by equation (5a), the conduction equation, or for small changes in temperature and distance

$$\frac{q}{A} = -\kappa \frac{\Delta T}{\Delta y} \Bigg|_{y=0} \quad . \tag{5c}$$

Since the temperature gradient at a wall is a continuous function, the known value of the gradient from the wall, represented by the first fringe shift can be used. This yields the following equations,

$$\frac{q}{A} = \frac{\kappa}{\Delta y} (T_w - T_i) \tag{16a}$$

or

$$\frac{q}{A} = \frac{\kappa \lambda_0 R T_i^2}{\Delta y L K P} \tag{16b}$$

The wall temperature is determined by means of the method illustrated in the discussion of the apparatus and the width of the first fringe shift can be measured on the interferograms.

III. EXPERIMENTAL APPARATUS

The experimental apparatus can be divided into three distinct parts. These consist of the table, the laser and its optical components, and the test section. A full view of the system is shown in Figure 2.

A. The Table.

In order to make a hologram free of any outside interference due to external motion, a vibration-free system is necessary. A large steel table weighing approximately 3/4 of a ton was placed on a 3/4 inch thick sheet of plywood which was in turn supported by six 5.60-12 rubber innertubes. The tubes served to damp out any vibration in the building. The apparatus was placed on the table top, thus avoiding interference due to external vibration.

B. The Laser and Optical Components

The laser used to make holograms was a Jodon Engineering model HN-1576 helium-neon gas laser which produces 20 milliwatts of power. The laser produces a monochromatic beam of light at a wavelength of 6328 angstroms. For purposes of reproduction on photographic film, both the above laser and a Jodon Engineering HN-50 helium-neon 50 milliwatt gas laser were used. This more powerful laser provided the higher intensity light necessary to get a clearer and brighter exposure.

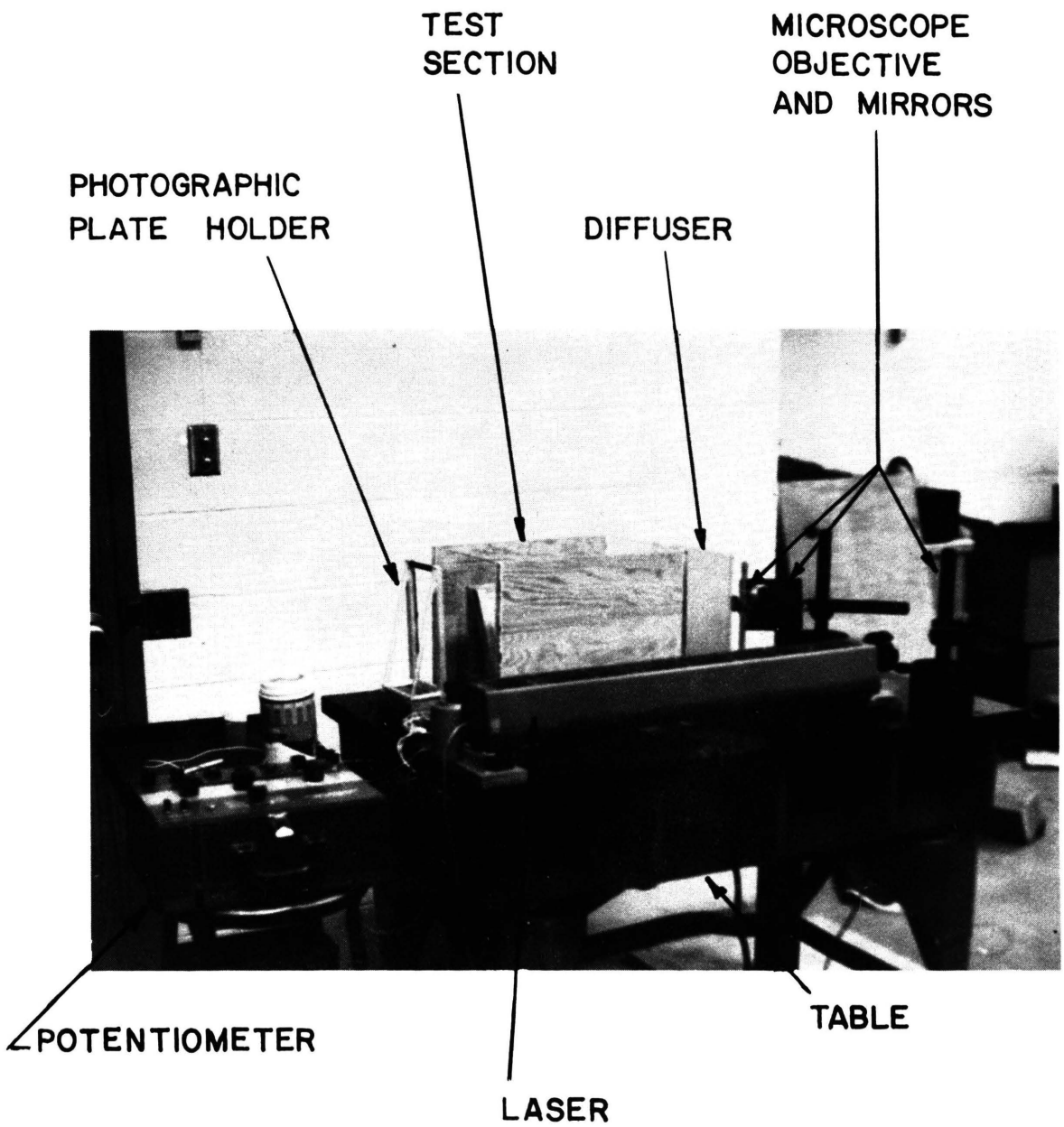

FIG. 2 SYSTEM APPARATUS

In order to obtain a beam large enough to make a successful hologram, a 100 power microscope objective lens was used. The lens was supported by a metal stand with a wooden base. Two front-silvered mirrors were used to direct the beam to the beam spreader. For reproductions, a 20 power objective lens was used to gain sufficient brightness. From the beam spreader, part of the beam was directed to a diffuser. The diffuser used was a 1/4 inch thick, 11 inch square plate of glass which was supported on two fiber stands and held in place by small bits of clay on the underside of the stands. In order to provide for the diffusion effect, one side was sand-blasted.

The photographic plates were held in place by a previously constructed assembly of hardwood and mounted on a metal base. It was designed to hold two 4 by 5 inch holographic plates necessary to obtain a full view of the boundary layer.

C. The Test Section

The plate used in the experiment was a 5/8 inch thick slab of aluminum, cut 12 inches long and 5-5/8 inches wide. Aluminum, because of its high thermal conductivity, was selected to help maintain a constant plate surface temperature. Eight feet of nichrome wire with a resistance of 5.6 ohms per foot was layed back and forth across the back of the plate as shown in Figure 3. In order to eliminate electrical short circuiting, a small coating of

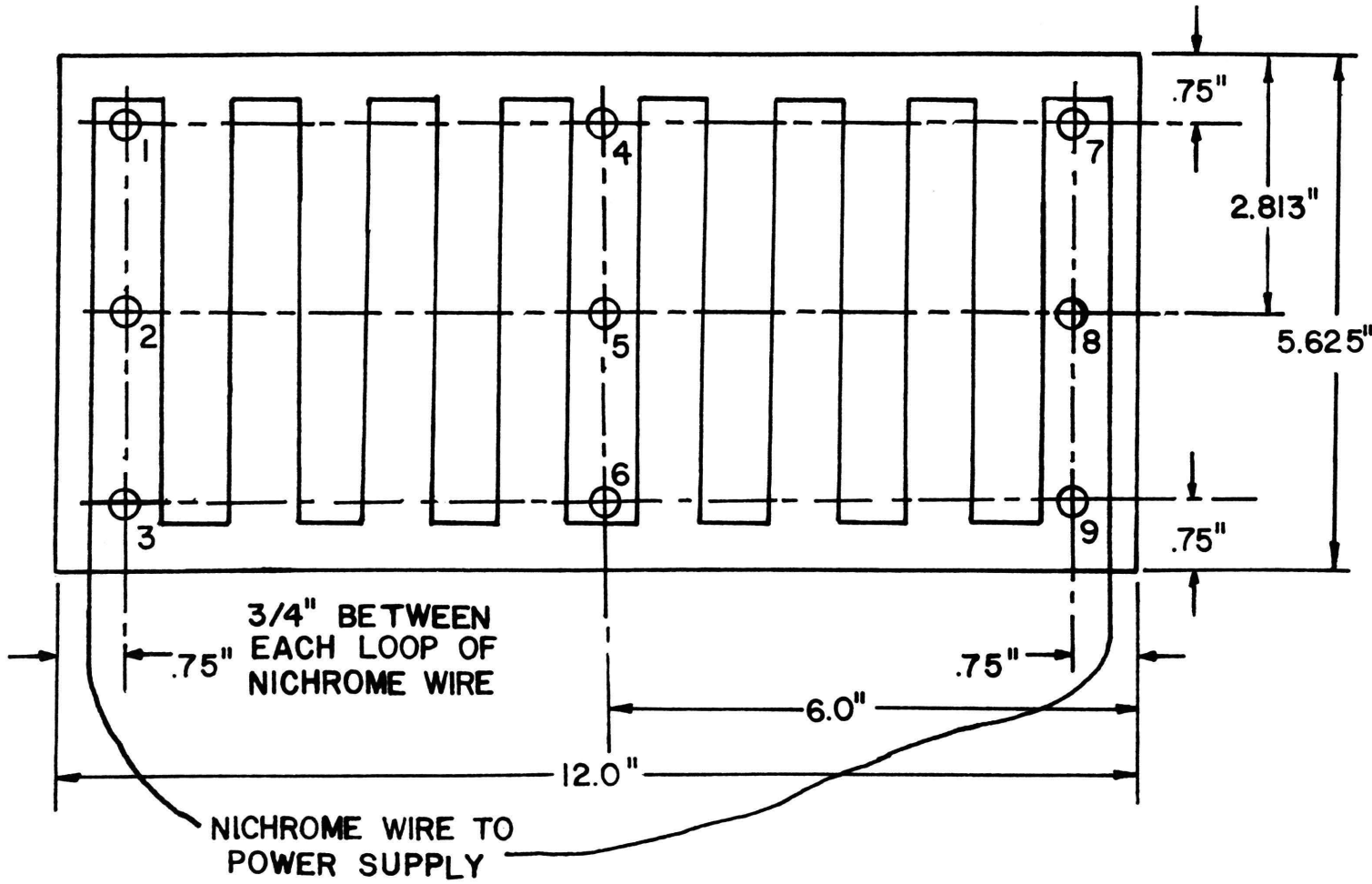

FIG. 3 NICHROME WIRE LAYOUT AND THERMOCOUPLE LOCATIONS

asbestos was applied to the plate surface. The nichrome wire was connected to a variable voltage rheostat in order to control the energy input to the system. Nine copper-constantan thermocouples were inserted into the back side of the plate as illustrated in Figures 3 and 4. Millivolt readings were obtained from a Leeds and Northrup potentiometer with an ice bath reference junction.

A wooden frame was constructed to serve as both an insulator for the sides, and a mold to contain the silicone rubber surrounding the back and sides of the plate. The silicone covered the sides and approximately one inch out from the back surface. This served to force most of the energy supplied out through the front surface of the plate. When placed in the vertical position, two small wooden legs and two large wooden struts were attached to support and anchor the plate and its frame to the table.

Several vertical black reference threads were spaced at 1/8 inch intervals in front of the plate surface. This provided a means for horizontal measurement in front of the plate. Vertical measurement was facilitated by placing straight pins in the silicone rubber at each end of the plate. Each pin was spaced at 1/2 inch increments from the bottom of the plate. Figure 5 shows a frontal view of the plate and its supporting structure.

In order to eliminate boundary layer fluctuations caused by room air currents, an enclosure was placed around the test plate. It was constructed of two plates of 1/4

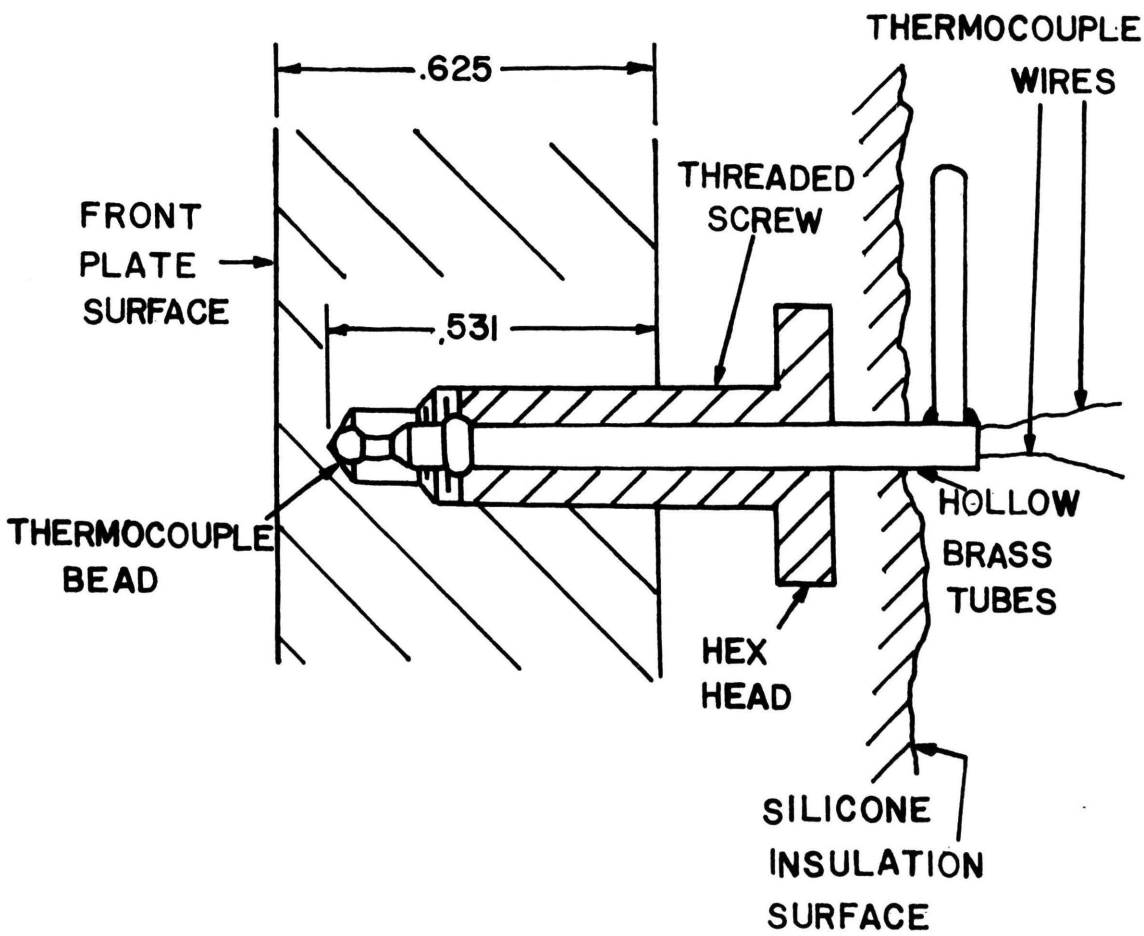

FIG. 4 THERMOCOUPLE INSTALLATION DETAIL

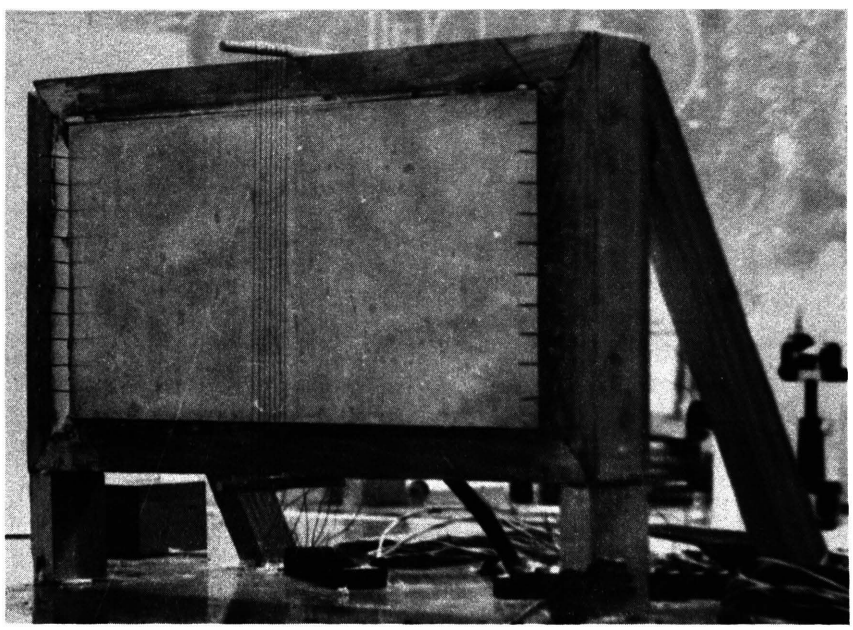

FIG. 5 TEST PLATE AND MOUNT

inch thick plywood. The enclosure was supported 3/4 of an inch above the surface of the table. This allowed sufficient air flow under the enclosure to feed the boundary layer at the plate surface. The enclosure also supported a movable thermocouple probe. The probe was positioned in the boundary layer to gather temperature data in the thermal boundary layer. The device consisted of a standard copper-constantan thermocouple contained in a section of 1/16 inch brass tubing. Guides of larger brass tubing were positioned in the wall of the enclosure facing the heated plate at one half inch vertical intermals. The thermocouple wires were bent in an L-shape, horizontal to the table surface and parallel to the plate surface, in order to avoid error measurements due to conduction along the thermocouple wires.

IV. TEST PROCEDURE

The method used to create the holograms was a double exposure technique. In Figure 6, a simple arrangement of the test section is shown and indicates the minimum requirements for the reference beam to approach the photographic plate. It must be remembered that the heated plate is surrounded by silicone-rubber insulation and a wooden frame. Since the reference beam may not touch the edge of the frame, it remains unaffected by the thin boundary layer. Other than this requirement, no positioning difficulties were experienced.

The first exposure was made at ambient conditions with all plate surface temperatures recorded by the nine thermocouples installed near the surface. At this point, the power supply was turned on and a period of 15 to 20 minutes was allowed to reach steady-state. With stability once more attained, a second exposure was made.

The holographic plates were developed for a period of six minutes in Kodak Microdol-X, then Kodak Indicator stop bath was used, and finally the plate was fixed in Kodak Rapid fixer for two minutes. Following a thirty minute wash, the plate was set aside to dry.

The temperature field was then probed while the plate was still at its second steady-state condition.

Reconstruction of the holographic images followed and was achieved by directing a laser beam through a 20 power

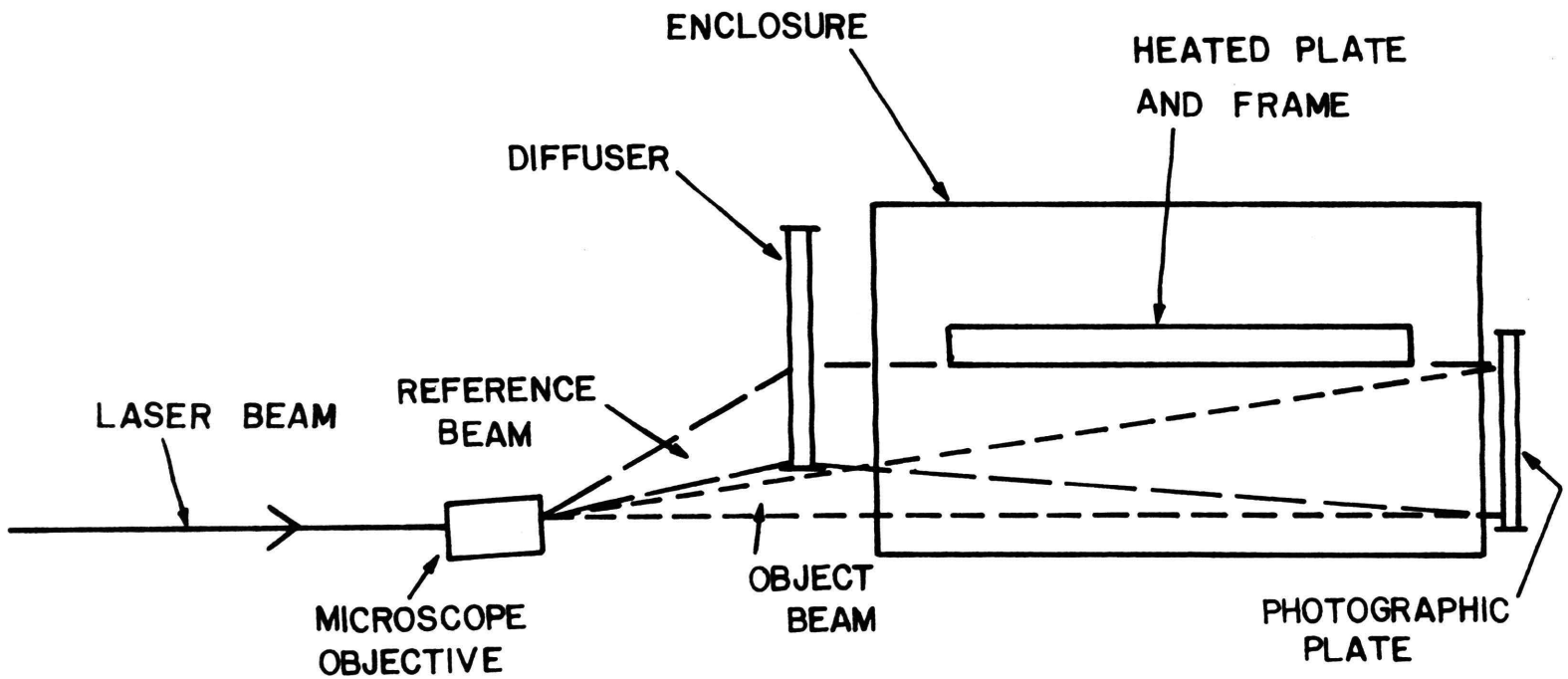

FIG. 6 SCHEMATIC OF THE APPARATUS

microscope objective lens. This provided a high intensity beam which made photographing the holograms a much simpler task. The photographs of the plates were exposed on Kodak Panatomic-X film using a Miranda Sensorex EE camera with time exposures of 60 to 120 seconds. A 50mm lens, a telephoto lens, and various lens extenders were used to make close-up exposures of particular points in the system. The film was processed and photographic prints were made using standard developing and printing procedures.

It must be remembered that the holograms made are three-dimensional in nature and if one wishes to view the fringe patterns along the edge of the plate, care must be taken to be sure the camera is properly positioned. If the camera is aligned incorrectly, the nearest fringe may be obstructed from view or the back edge of the plate will appear as an extra fringe.

Due to the height of the holographic plate, it is difficult to obtain a complete picture of the plates without great loss of detail. The best solution is to make a series of exposures with the camera centered at a different vertical position along the plate. Three picture positions allowed an overlapping of certain positions so findings could be readily compared. For each case the camera was positioned at one inch, two and one half inch, and four and one half inch marks.

V. RESULTS

Figures 7 through 10 illustrate the boundary layers of the three experiments conducted during this study. Figures 7 and 8 show conditions at the same wall temperature but at different ambient air temperatures. Figure 9 is an example of the boundary layer formation for a plate surface temperature of 125°F. In the 125°F interferogram, fringe spacing is small which makes the temperature field hard to analyze without resorting to magnified photography.

Corresponding experiment data for Figures 7 through 10 are contained in Tables I, II and III. All thermocouple probe data are listed and values correspond with the grid system on Figures 7 through 10. Plate surface temperatures are included with the average temperature being a simple arithmetic mean.

Figures 11 through 13 illustrate a graphical comparison of the visual and theoretical boundary layer, equation (4). In each case there is a reasonable correlation between theory, equation (4), and the interferogram boundary layers. For each plate, the largest disagreement with theory occurs toward the top of the plate. This is especially evident in Figure 11 where the boundary layer appears to be turning toward the plate surface. This can be explained by the fact that the theory was developed for a plate that is vertically semi-infinite. Since the experimental plate is finite in height, the atmosphere above the plate will cause a net cooling effect causing shrinkage of the boundary layer.

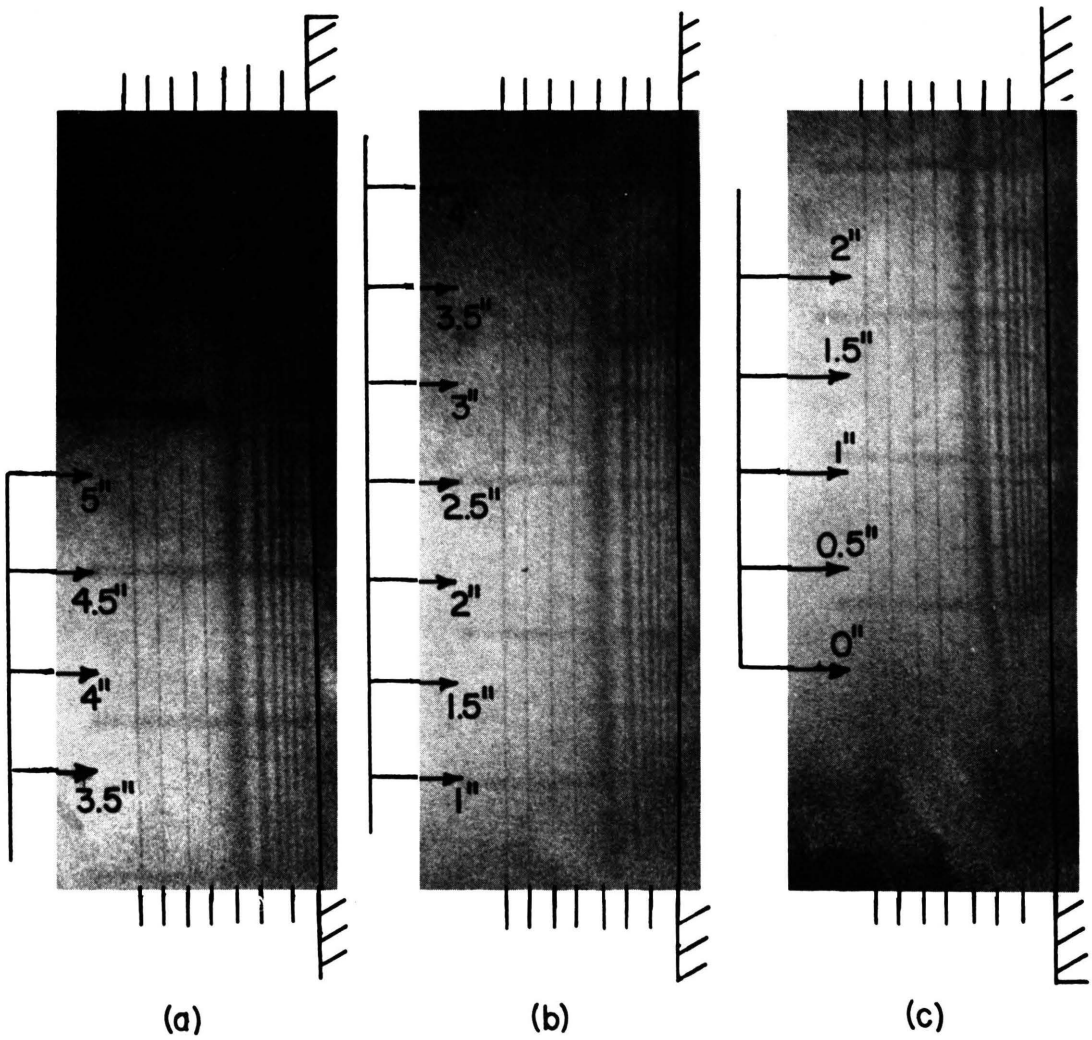

FIG. 7 INTERFEROGRAM OF FIRST 100°F PLATE

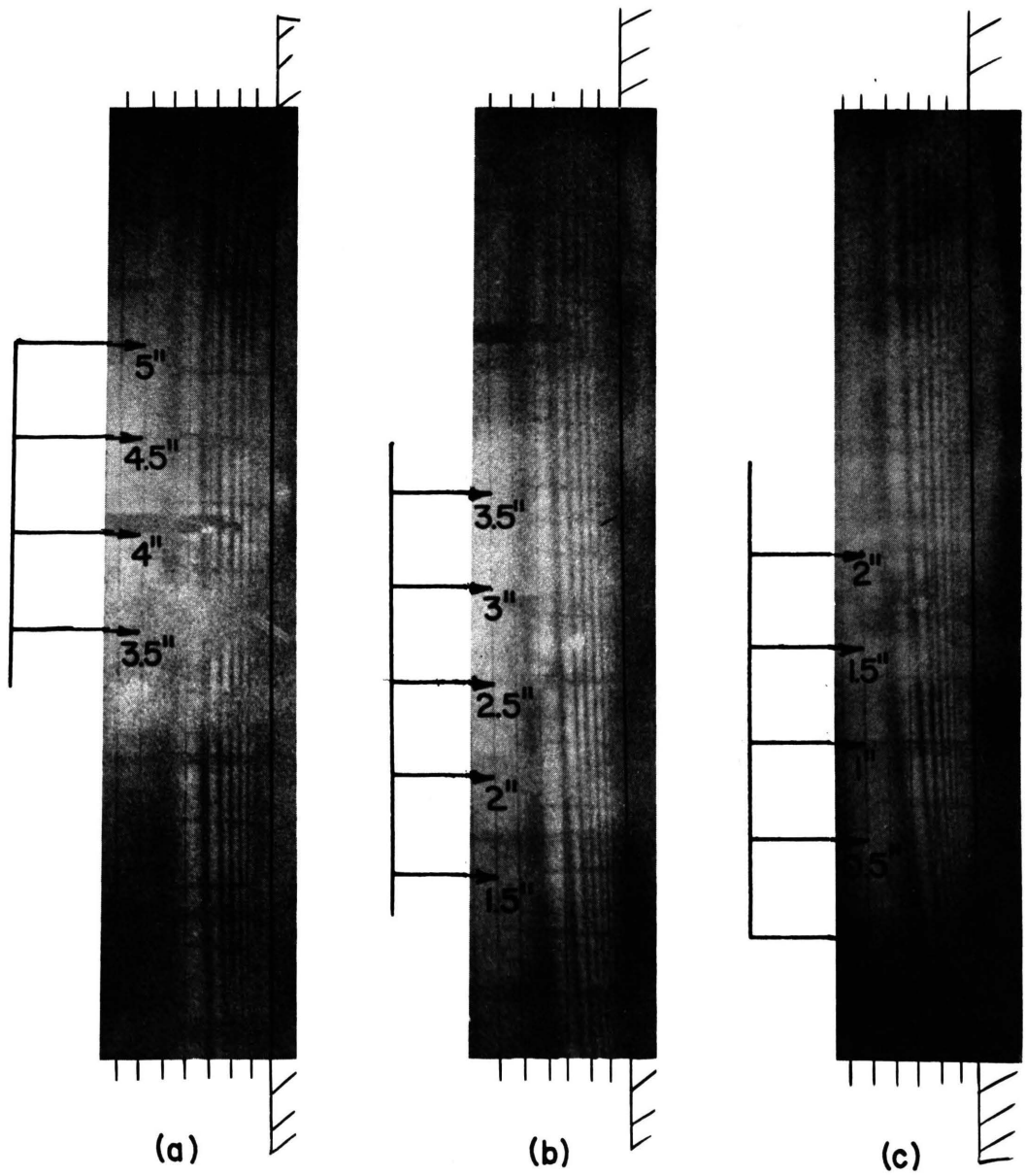

FIG. 8 INTERFEROGRAM OF SECOND 100°F PLATE

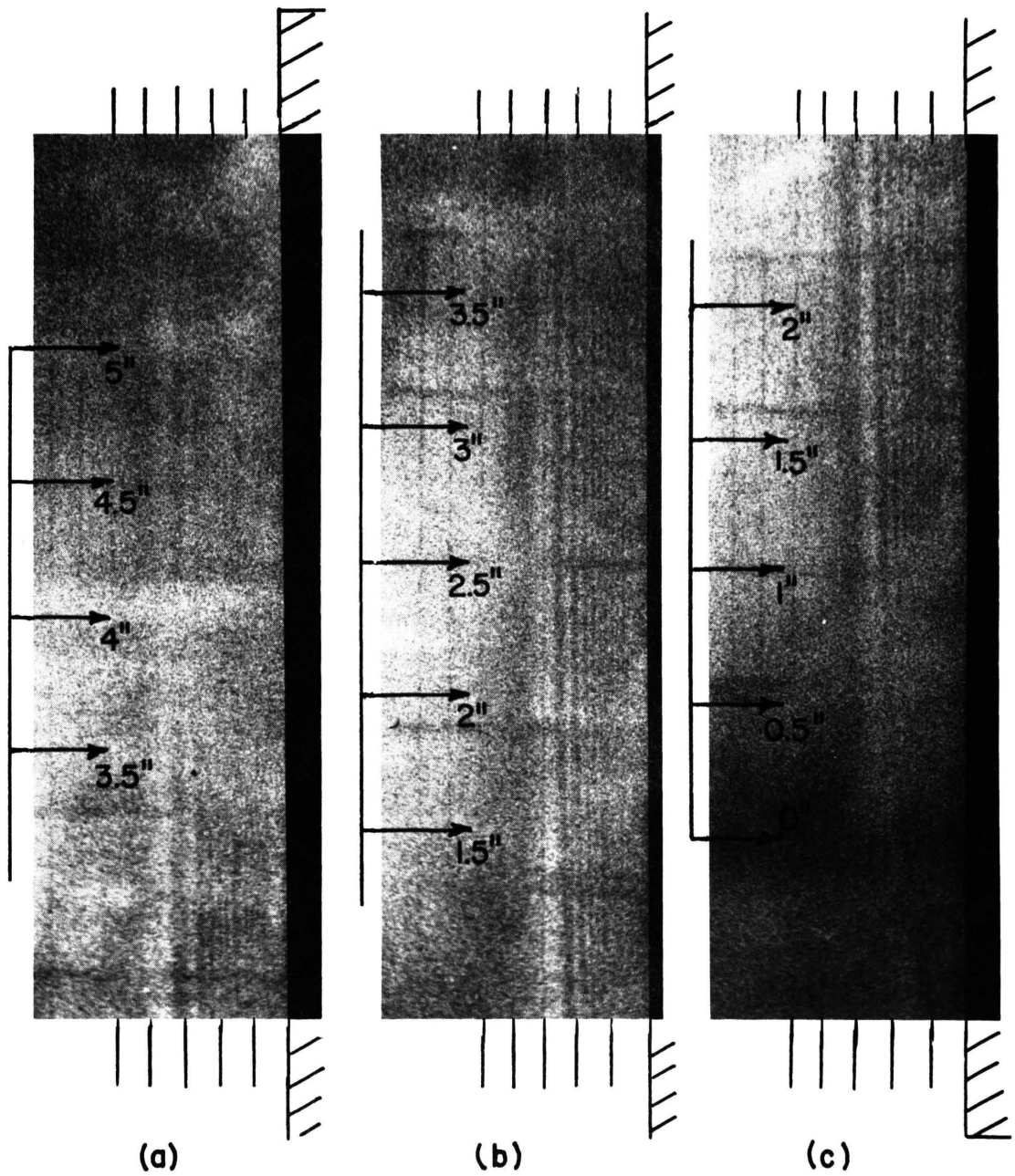

FIG. 9 INTERFEROGRAM OF 125°F PLATE

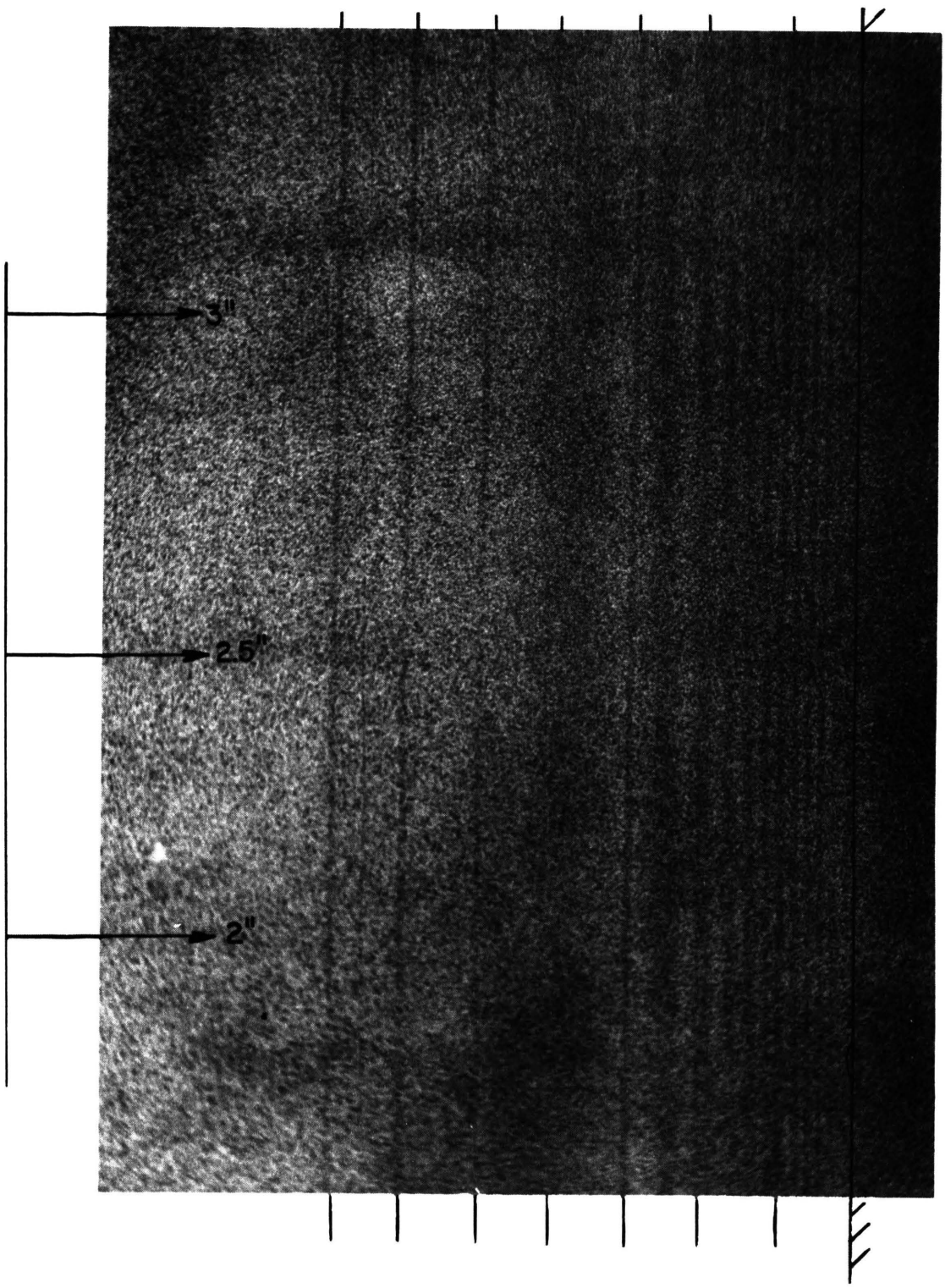

FIG. 10 CLOSE-UP OF FIGURE 9b

TABLE I. Thermocouple Data for First 100°F Plate

Plate temperatures - °F

Thermocouple #:

1	2	3	4	5	6	7	8	9
100.3	100.4	100.2	100.2	100.3	100.3	100.1	100.2	100.2

Average plate temperature = 100.2

Ambient air temperature = 74.3

Thermocouple probe data - °F

	Horizontal Position (in)			
Plate Height (in)	.125	.250	.375	.500
0.5	83.9	79.3		
1.0	85.6	80.4	78.4	
1.5	85.7	82.0	78.7	
2.0	87.6	82.1	79.6	
2.5	86.0	81.6	79.4	78.0
3.0	87.7	82.8	80.3	78.8
3.5	88.2	83.6	80.3	78.7
4.0	88.0	83.8	81.3	80.1
4.5	88.3	83.6	81.5	80.3
5.0	86.8	83.3	80.6	78.6

TABLE II. Thermocouple Data for Second 100°F Plate

Plate thermocouples - °F

Thermocouple #:

1	2	3	4	5	6	7	8	9
100.2	100.5	100.3	100.4	100.4	100.4	100.2	100.3	100.3

Average plate temperature = 100.3

Ambient air temperature = 70.7

TABLE III. Thermocouple Data for 125°F Plate

Plate temperature - °F

Thermocouple #:

1	2	3	4	5	6	7	8	9
125.9	125.8	125.6	125.6	125.6	125.6	125.3	125.5	125.5

Average plate temperature = 125.6

Ambient air temperature = 75.7

Thermocouple probe data - °F

	Horizontal Position (in)			
Plate Height (in)	.125	.250	.375	.500
0.5	80.9	77.6		
1.0	83.7	79.0		
1.5	86.3	81.1	77.7	
2.0	88.6	80.4	77.8	
2.5	89.5	80.5	78.0	
3.0	90.9	82.3	79.1	
3.5	91.3	83.3	80.4	79.1
4.0	96.1	81.9	80.1	78.3
4.5	99.3	87.2	80.4	78.6
5.0	96.7	87.4	81.0	79.8

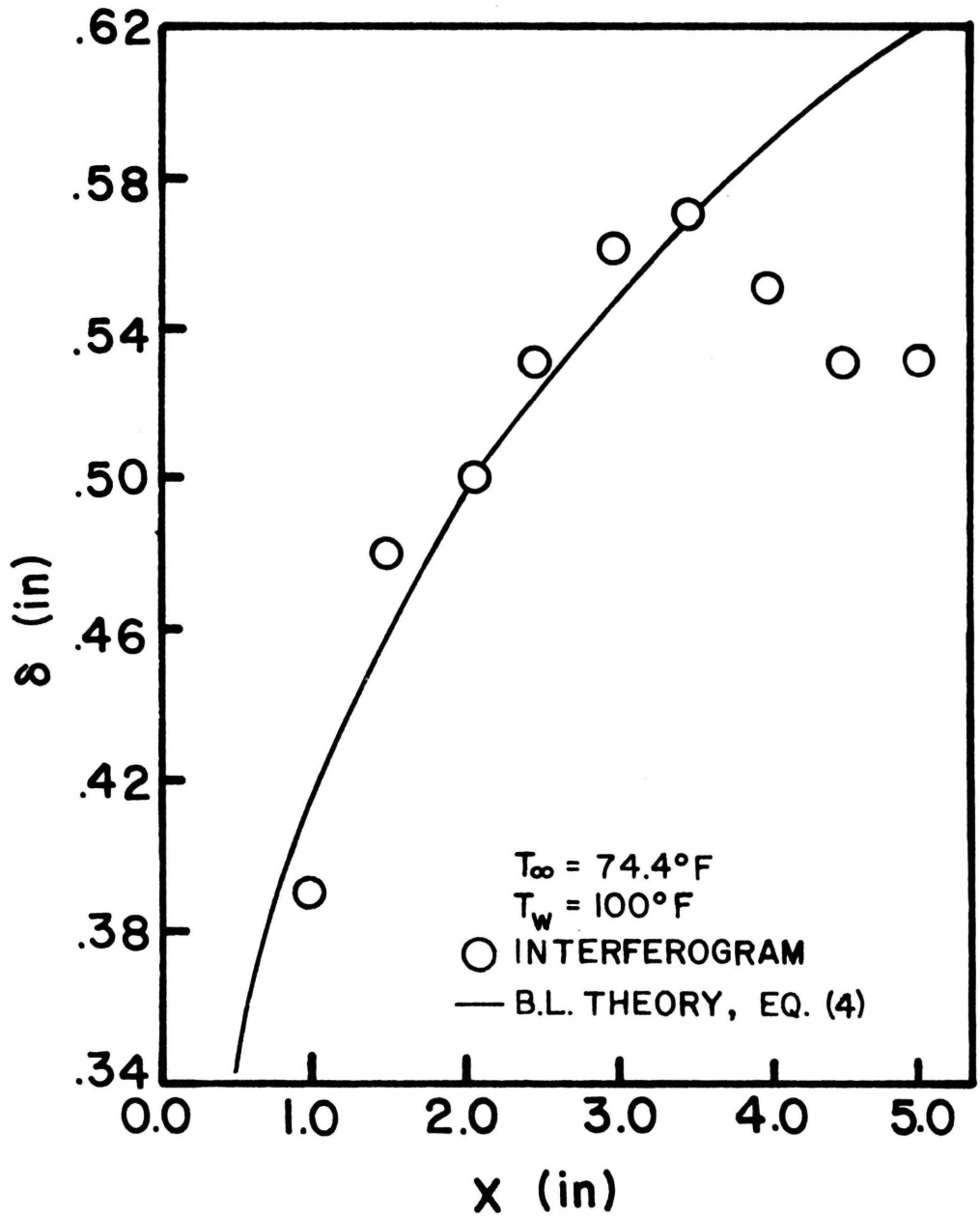

FIG. 11 BOUNDARY LAYER THICKNESS FOR AIR (EXP. 1)

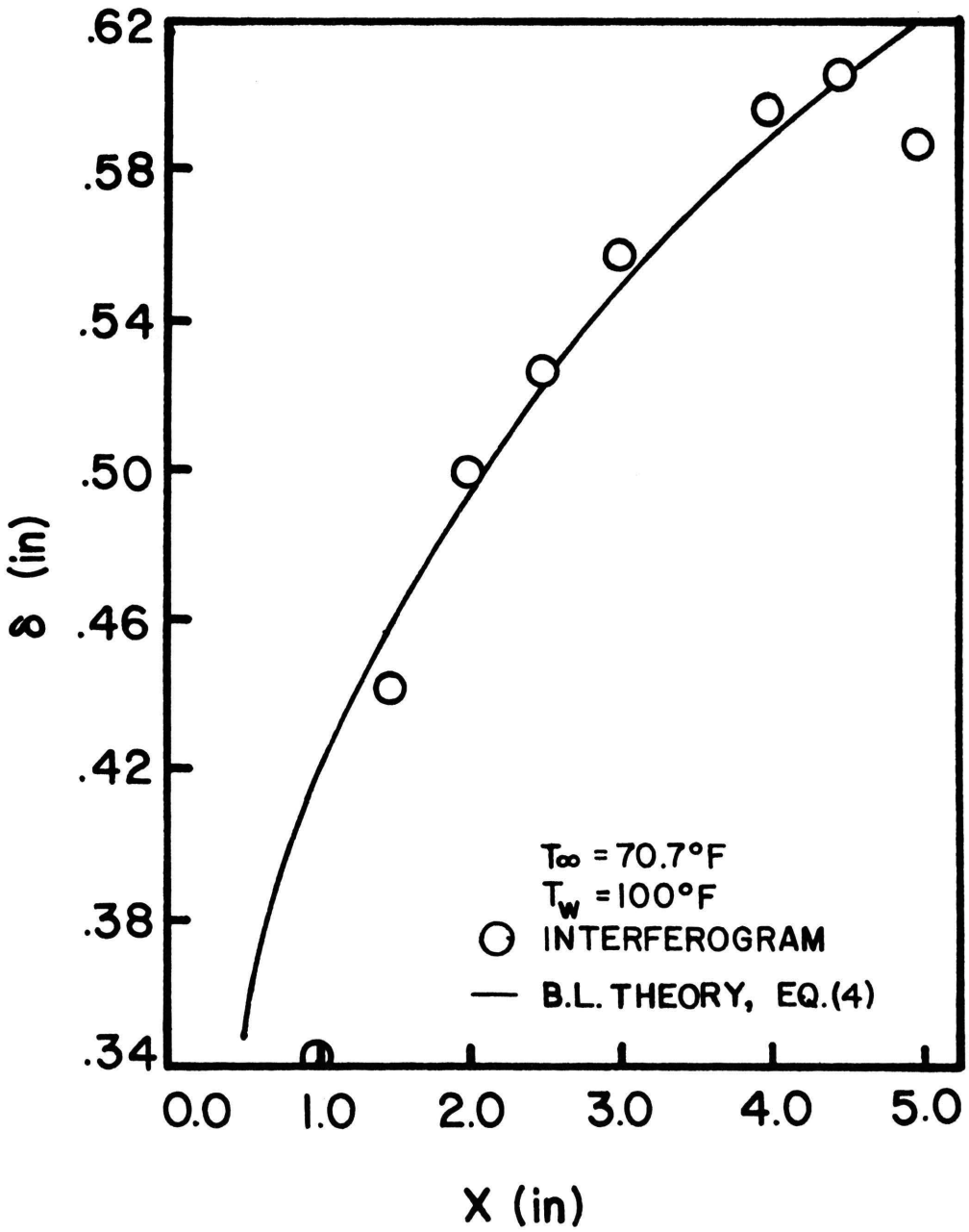

FIG. 12 BOUNDARY LAYER THICKNESS FOR AIR (EXP. 2)

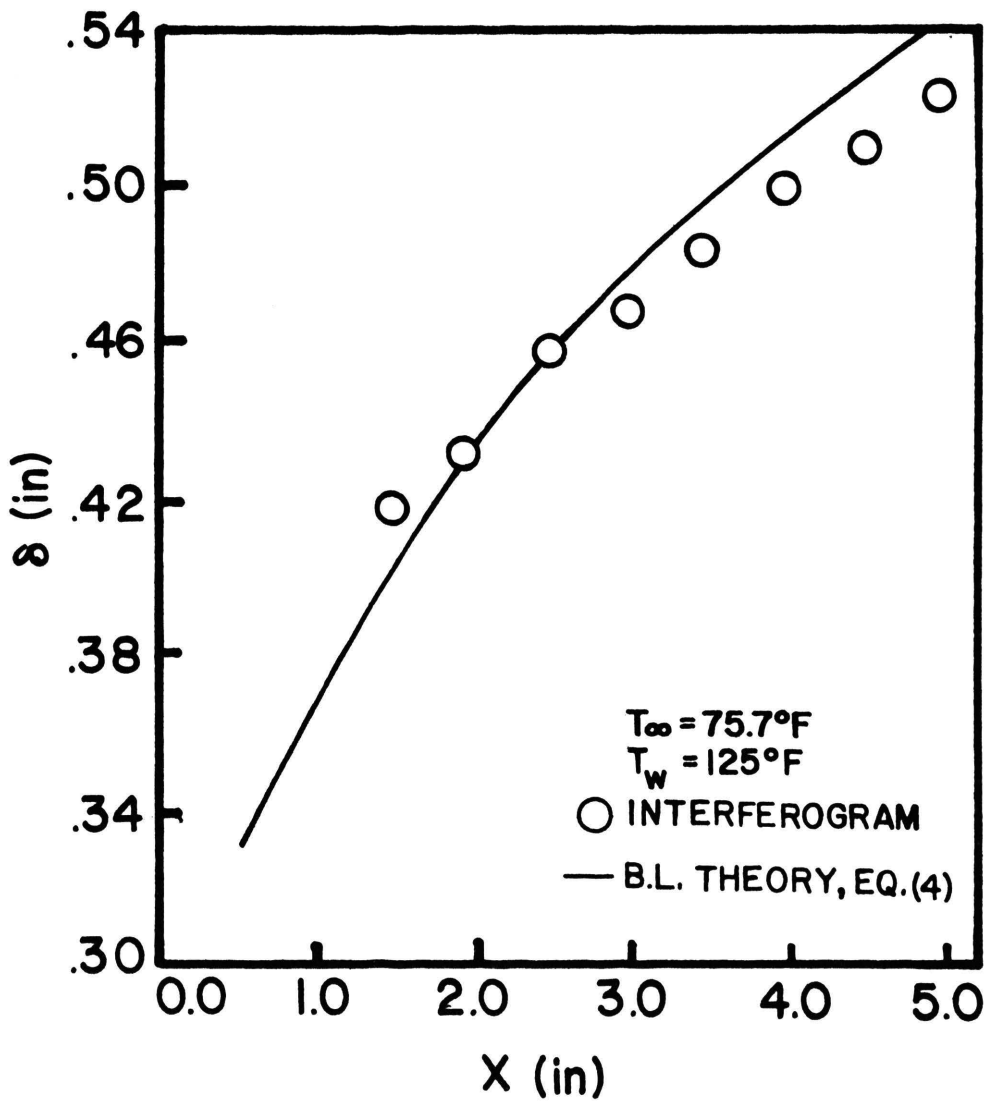

FIG. 13 BOUNDARY LAYER THICKNESS FOR AIR (EXP. 3)

In order to assure the accuracy of the boundary layer profile, an analysis was conducted to determine the temperature gradient in the silicone rubber. The silicone rubber was considered to be a long fin with the temperature at the end to be essentially the ambient air temperature. Solution equations for this problem can be found in Holman [9] or any other heat transfer text book. The calculation indicated a temperature field a distance of .579 inches before the leading edge of the plate. Assuming that the boundary layer started approximately .50 inches from the leading edge of the plate, a value for the boundary layer thickness was measured from the photographs and the .50 inches was added to the height to adjust the vertical position. The distance was used to make vertical adjustments to calculate the boundary layer thickness.

Figures 14 through 16 show the temperature profiles in the boundary layer. The calculations were made two and one-half inches above the leading edge of the plate. In each case, the points represent respective fringe temperatures and their positions in the boundary layer. In the first approach, fringe temperatures were calculated using equation (14) and starting from the ambient air and working in toward the plate. A second method started at the wall surface and worked out toward the ambient air. The values for boundary layer temperature calculated using the second method indicates there is cooling occuring in the boundary layer, which is impossible. This illustrates

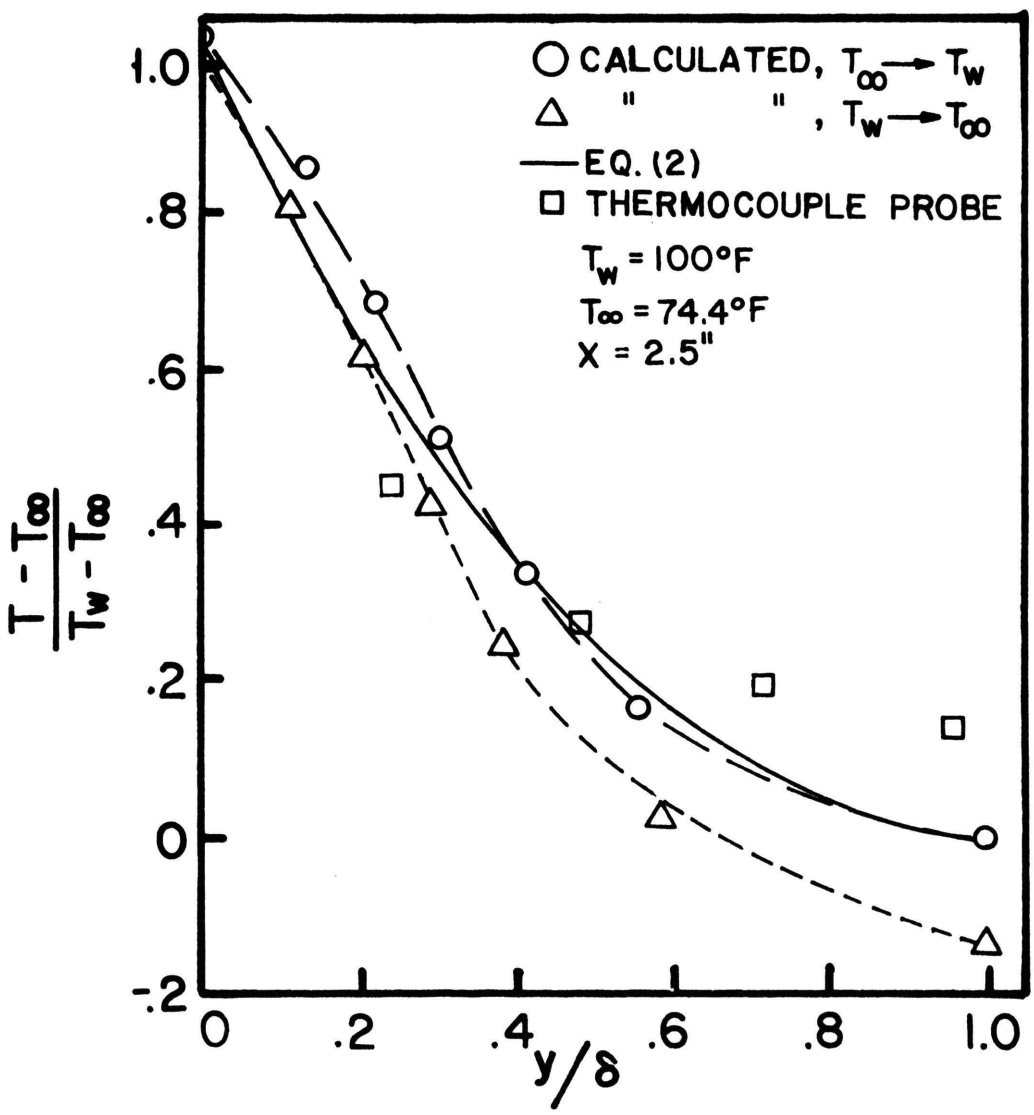

FIG. 14 AIR TEMPERATURE PROFILE IN THE BOUNDARY LAYER (EXP. 1)

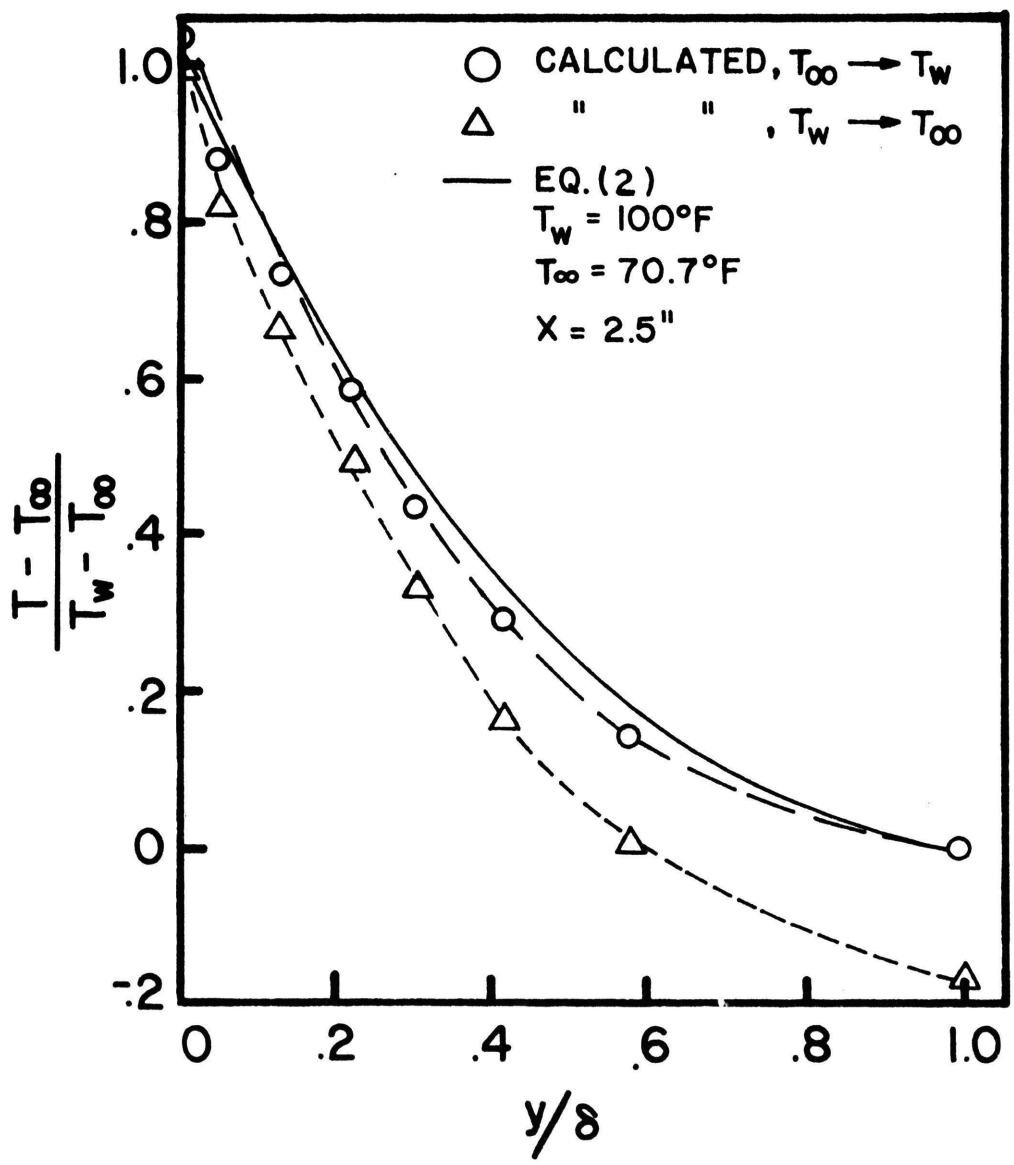

FIG. 15 AIR TEMPERATURE PROFILE IN THE BOUNDARY LAYER (EXP. 2)

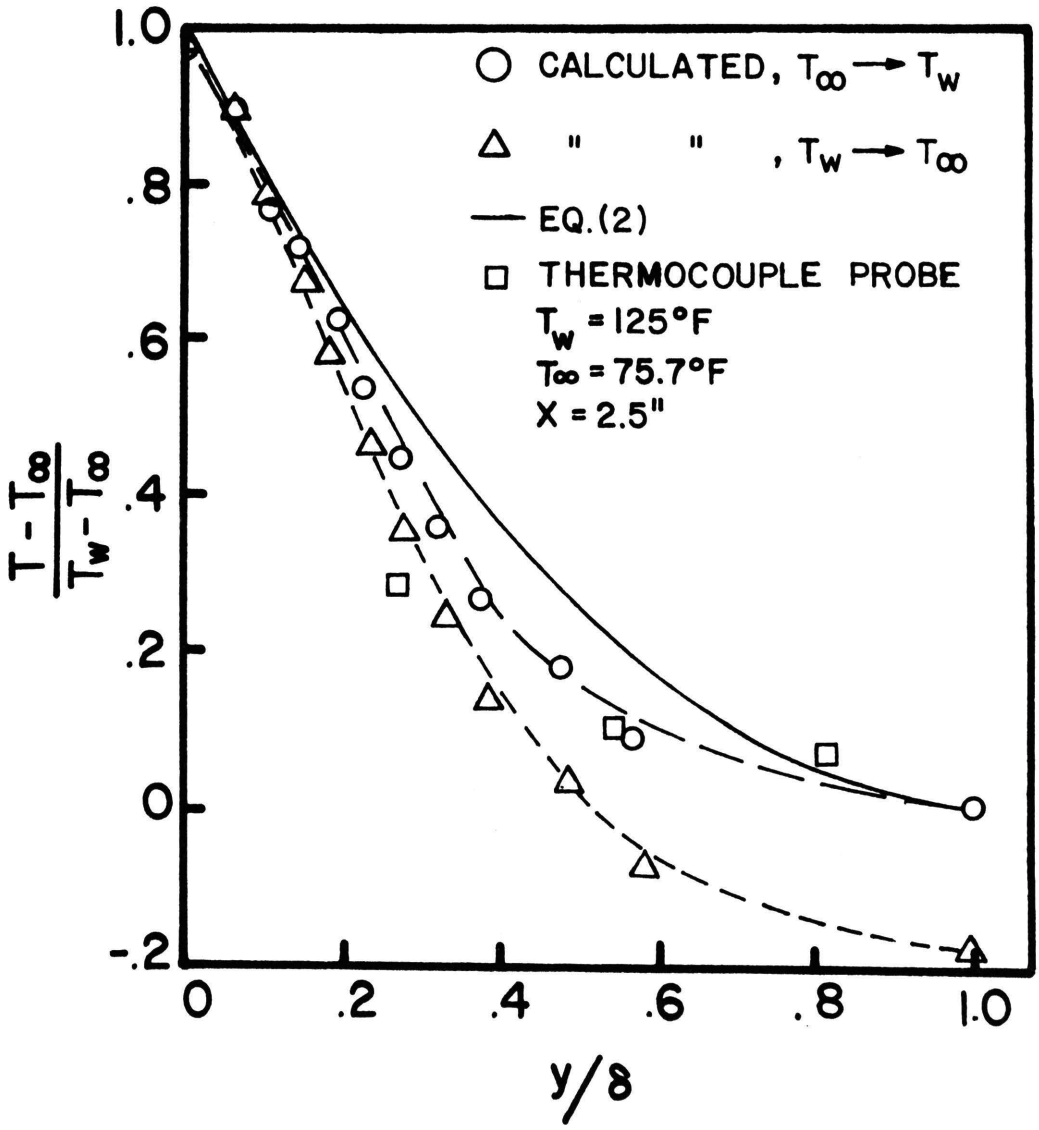

FIG. 16 AIR TEMPERATURE PROFILE IN THE BOUNDARY LAYER (EXP. 3)

an importance in the procedure used to extract data from the interferogram. The major reason for the variation is that if T_i in equation (14) is assumed to be T_w, then the inherent experimental error, due not only to small inaccuracies in the thermocouple, but also to variances in plate surface temperatures is magnified because T_i is squared. Experimental error is presented in an error analysis presented in Appendix I.

Thermocouple data are included in Figures 14 and 16, but are less descriptive of the temperature profile than optical measurements. The thermocouple readings were poor near the plate surface where the cross-section of the thermocouple bead overlapped many fringes and thus was at best giving an average value which may best represent considerable experimental error.

Figures 17 through 19 are comparisons of the heat transfer as predicted by the boundary layer theory, equation (5b) and equation (16b) from optical theory. In all cases, and in particular, around the vertical center of the plate, both theories show close agreement. The largest deviation occurs toward the upper and lower ends of the plate where there is heat transfer in the silicone rubber. A portion of this deviation is the result of poor image quality at these stations on the interferograms. The most pronounced illustration is shown at the top of the 125°F plate, Figure 10a. In this case, it was barely possible to obtain the boundary layer thickness, much less the

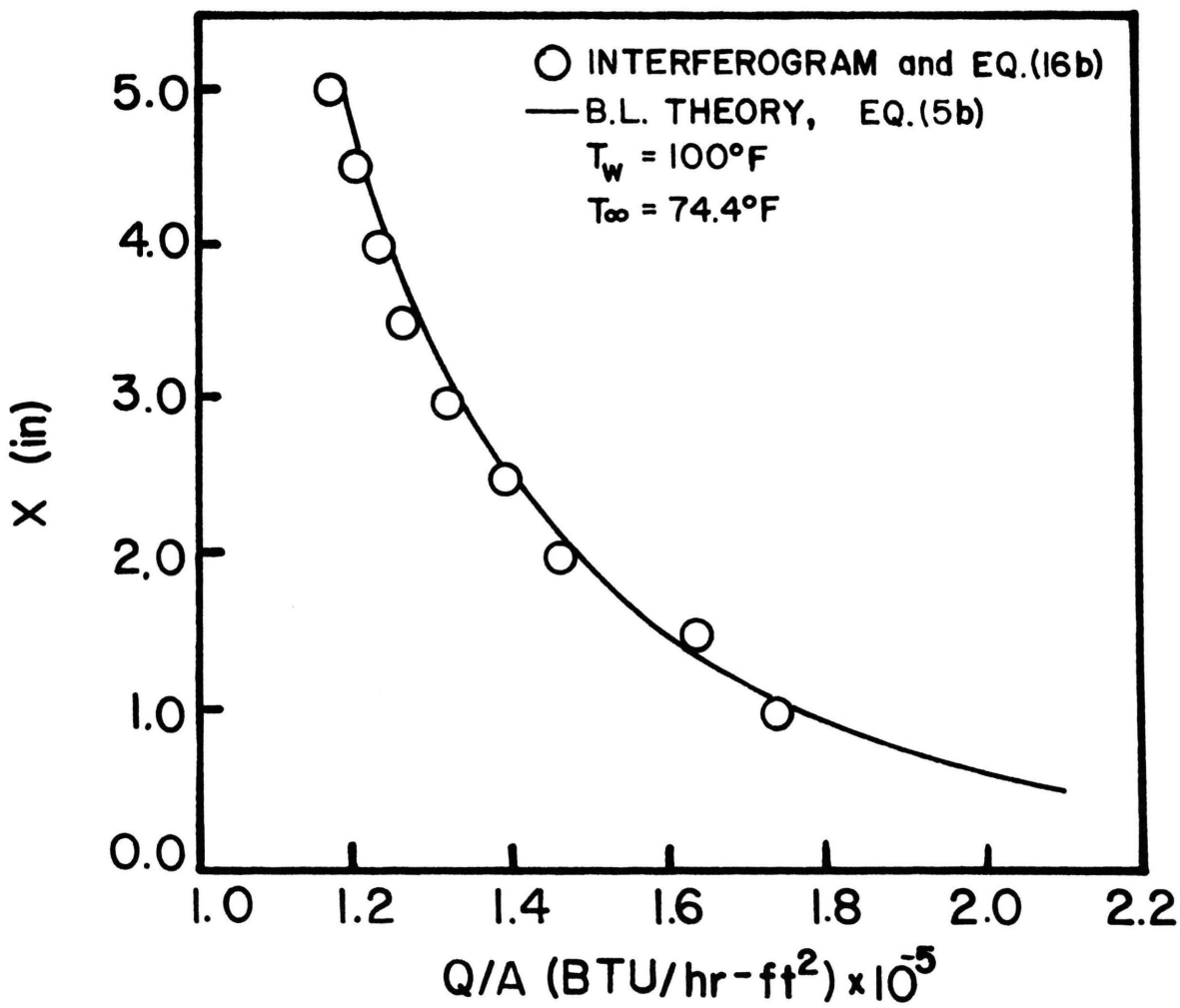

FIG. 17 HEAT TRANSFER DATA (EXP. 1)

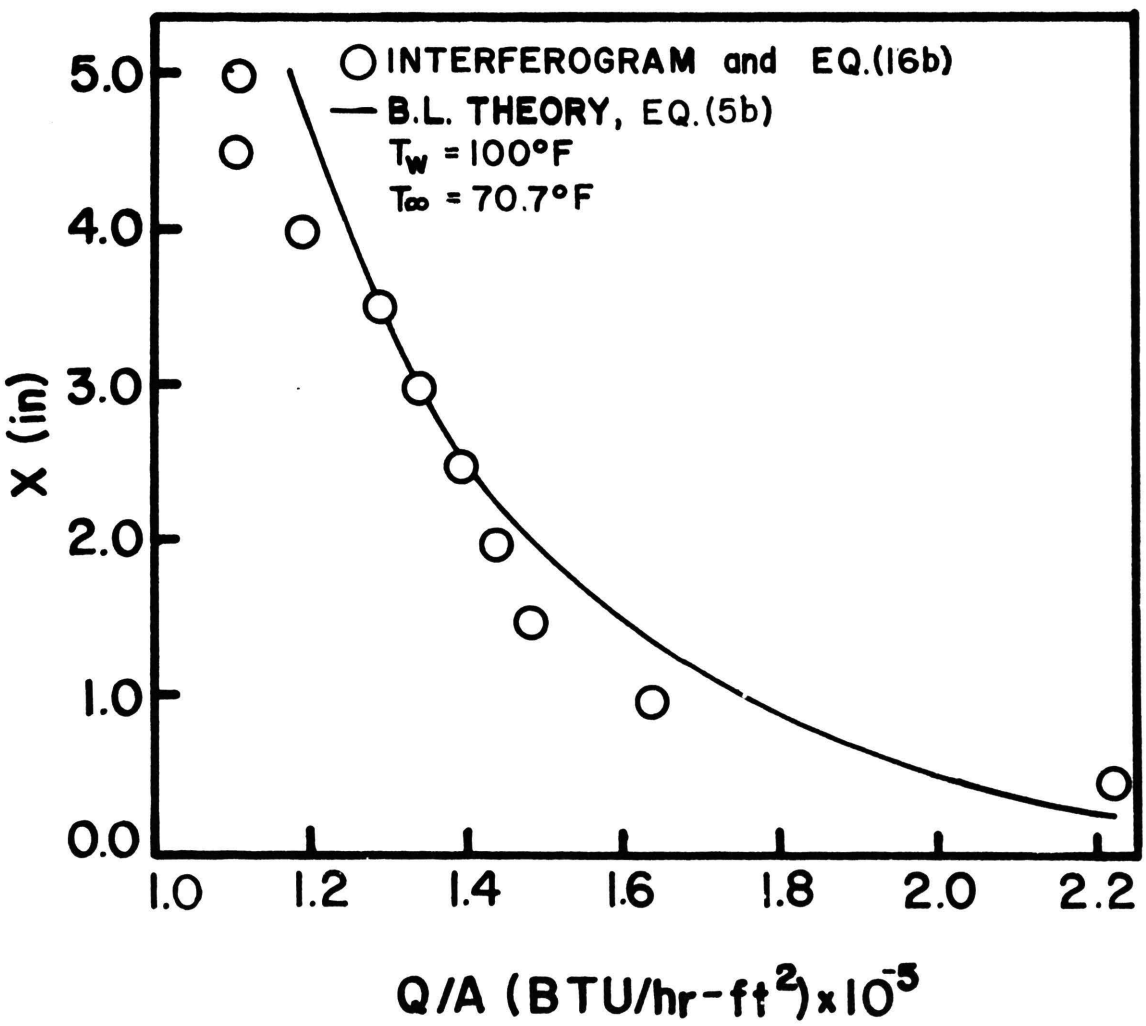

FIG. 18 HEAT TRANSFER DATA (EXP. 2)

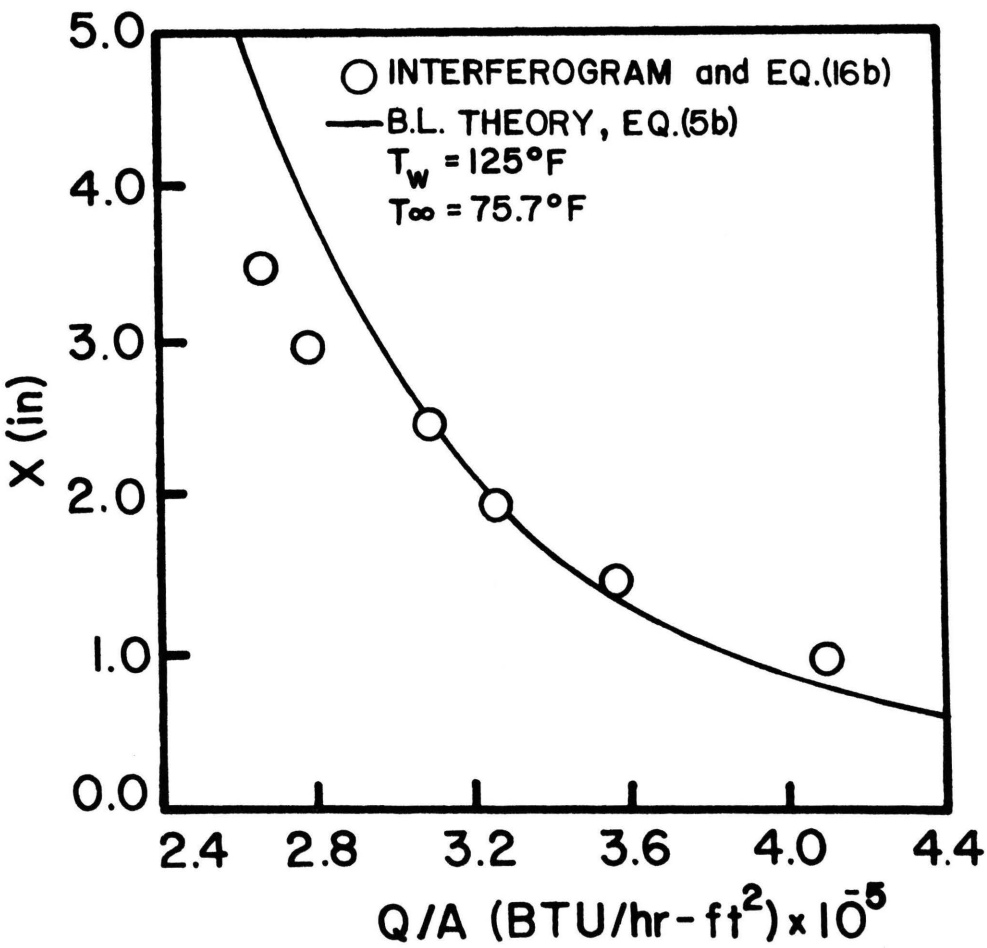

FIG. 19 HEAT TRANSFER DATA (EXP. 3)

distance of the first fringe shift. Hence, all heat transfer data above 3.5 inches is not being considered. One important point, which eases calculation of heat transfer, is that, because the visual appearance of linearity of the fringe system throughout the first few fringe shifts, one may use as many shifts as is deemed necessary over the linear range to obtain a value for the heat transfer. For example, four fringe shifts were used in the calculation of the heat transfer from the 125°F plate.

The results given by Figure 20 show a comparison of the number of fringes observed to the number predicted by optical theory. It can be noted that although there were two plates with the same surface temperature, the interferograms of these two plates show 6.0 and 7.0 fringes, respectively. The appearance of the added fringe is due to the lower air temperature, which caused the ratio of T_w-T_∞/T_∞^2 to increase, further causing an increase of as much as one fringe shift, despite a difference of only 3.7°F. This is an excellent example of the sensitivity of the optical holographic interferometer. The difference in theoretical and observed fringes will be discussed in Appendix I in an attempt to further demonstrate that the Gladstone-Dale optical theory equations yield results well within the error band of the experiment.

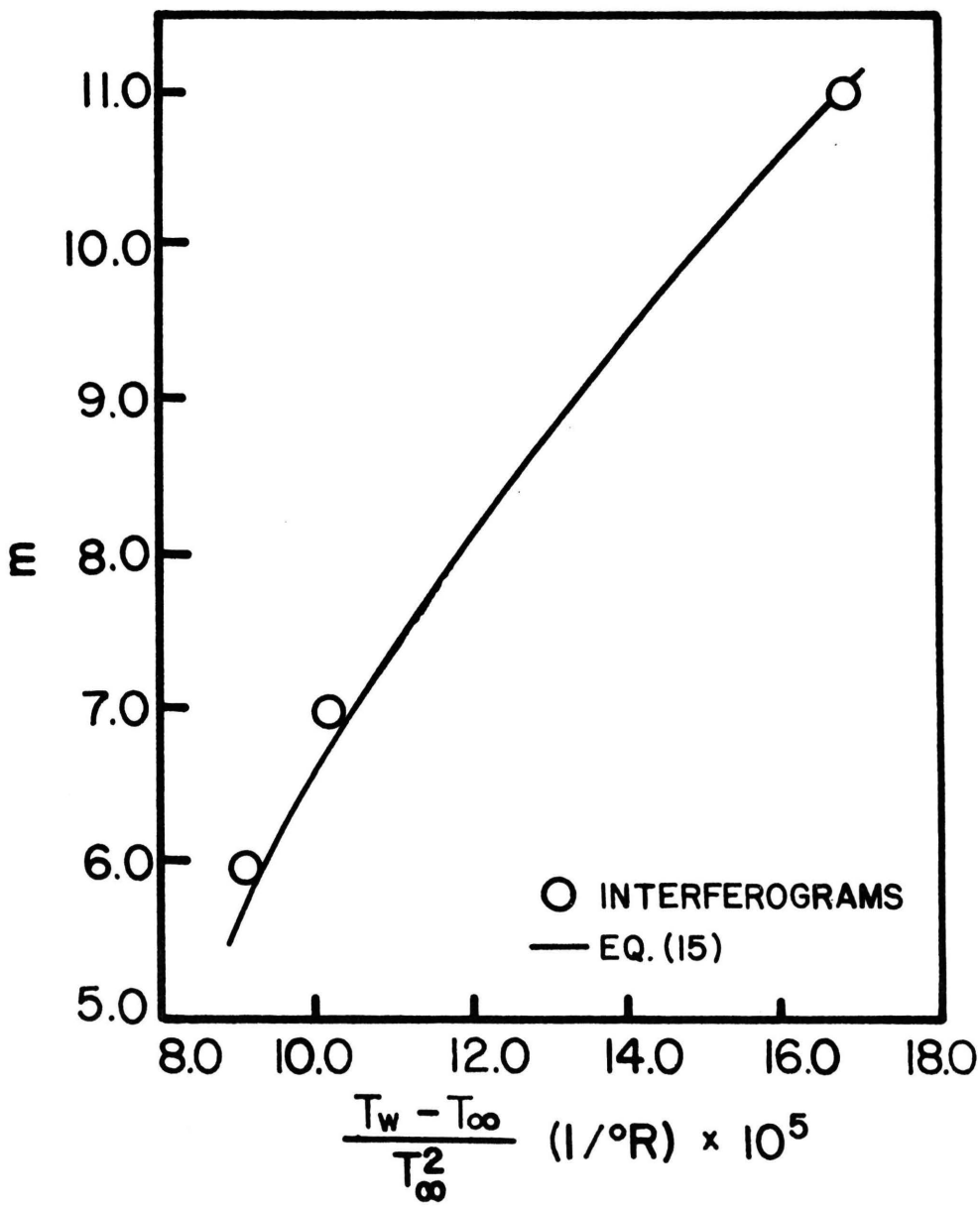

FIG. 20 NUMBER OF FRINGES

VI. CONCLUSIONS

The laser holographic interferometer technique was shown to be an accurate method for determining heat transfer conditions in a boundary layer. The reasonable agreement between the interferometer results with the established integral approximation theory is shown. The interferometer data yielded results which were accurate within the estimated deviations caused by the experimental test surface. These deviations are discussed in Appendix I.

By knowing the temperature at any given point in the fringe system, all other temperature data can be calculated through a set of simple and straightforward equations.

This establishes an experimental technique which may be superior to all other in determining two-dimensional temperature fields in a complex system.

The three-dimensional aspect, ease of set up, nondependence on high quality optics, and low cost support the opinion that the laser holographic interferometer system is equal to or better than any other method available for the measurement of temperature fields in a gas.

BIBLIOGRAPHY

1. Thomson, R. K., Laser Interferometric Holography Investigation of Free Convection About a Vertical Plate of Non-Uniform Temperature. UMR Thesis, 1971.

2. Reifel, A., Analysis of Interferometric Holography in Temperature Measurement. UMR Thesis, 1973.

3. Zinnes, A. E., "The Coupling of Conduction With Laminar Natural Convection From a Vertical Flat Plate With Arbitrary Surface Heating," Transaction of the ASME Journal of Heat Transfer, Aug. 1970, Pages 528-535.

4. Hauf, W. and U. Grigull, "Optical Methods in Heat Transfer," Advances in Heat Transfer, Vol. 6, New York: Academic Press, 1970.

5. Heflinger, L. O., R. F. Wuerker, and R. E. Brooks, "Holographic Interferometry," Journal of Applied Physics, Vol. 37, No. 2, Feb 1966, Pages 642-49.

6. Brooks, R. E., "New Dimension For Interferometry," Electronics, Vol. 40, No. 10, May 15, 1967. Pages 88-93.

7. Smith, H. M., Principles of Holography, New York-Wiley-Interscience, 1969.

8. Reisbig, R. L., "A Temperature Interferometer Using Laser Holography," ISA Trans., Advances in Instrumentation, Vol. 27, Part 2, 1972.

9. Holman, J. P., Heat Transfer. New York: McGraw-Hill, 1968.

10. Longhurst, R. S., Geometrical and Physical Optics. London: Longmans, Green and Company, 1957.

VITA

Richard Michael Quinlisk was born on March 16, 1949 in St. Louis, Missouri. He received his elementary education in St. Louis and Florissant, Missouri, and his secondary education in Florissant, Missouri. His college education was undertaken at the University of Missouri-Rolla in Rolla, Missouri where he received a Bachelor of Science Degree in Mechanical Engineering in December of 1971.

During his college education he has become a member of Honorary Society of Pi Tau Sigma and of the professional society of the American Society of Mechanical Engineers.

He has been enrolled in the Graduate School of the University of Missouri-Rolla since January 1972 and has been supported by a teaching assistantship granted by the Mechanical Engineering Department for the period of January, 1972 to May, 1973.

APPENDICES

I. ERROR ANALYSIS

In order to demonstrate the validity of the theory developed for this interferometer based on the Gladstone-Dale law, some form of analysis must be made of the inherent error in the experiment.

From equation (15), the fringes predicted can be expressed as a function of four variables,

$$m = m\ (L,P,T_w,T_\infty)\,. \tag{17}$$

To determine the variation in m as a result of experimental error can be expressed in terms of a total differential

$$dm = \frac{\partial m}{\partial L}\,dL + \frac{\partial m}{\partial p}\,dP + \frac{\partial m}{\partial T_w}dT_w + \frac{\partial m}{\partial T_\infty}\,dT_\infty. \tag{18}$$

For this analysis dP will be considered as negligible when compared with other estimated errors. Equation (15) will yield the following expressions for the partial derivatives,

$$\frac{\partial m}{\partial L} = \frac{\kappa P}{\lambda_o R} \cdot \frac{T_w - T_\infty}{T_\infty^{\,2}} \tag{19a}$$

$$\frac{\partial m}{\partial T_w} = \frac{LKP}{\lambda_o R}\quad \frac{1}{T_\infty^{\,2}} \tag{19b}$$

$$\frac{\partial m}{\partial T_\infty} = \frac{LKP}{\lambda_o R}\quad \left(\frac{2T_w}{2_\infty^{\,2}} - \frac{3}{T_\infty^{\,2}}\right) \tag{19c}$$

With these partial derivatives established, values for the three estimated errors must be calculated. For the error in the ambient air measurement, the copper constantan

thermocouple was calibrated against a quartz thermocouple. This value is given in Table IV. The error in plate temperature measurements was based on both thermocouple error and variations in measured surface temperature. The basis for error in the length was the difference in actual length and the length "seen" by the interferometer due to end effects such as heating of the silicone rubber insulation. Therefore, the estimated errors may be written as follows,

$$dT_\infty = dT_{t.c.} \tag{20a}$$

$$dT_w = dT_{t.c.} + dT_{p.t.} \tag{20b}$$

$$dL = L_{t.} - L \tag{20c}$$

This gives a total expression for dm as

$$dm = \frac{\kappa P}{\lambda_0 R}\left[\left(\frac{T_w - T_\infty}{T_\infty^2}\right)(L_{t.} - L) + \frac{L}{T_\infty^2}\left(dT_{t.c.} + dT_{p.t.}\right)\right.$$

$$\left. + L\left(\frac{\partial T_w}{T_\infty^3} - \frac{3}{T_\infty^2}\right) dT_{t.c.}\right] \tag{21}$$

which is also the estimated deviation in the number of theoretical and observed fringe shifts,

$$dm = m_t - m_0 \tag{22}$$

From Figure 19, the value for m_t and m_0 can be obtained. In all cases, difference represented in equation (22) was well within the maximum predicted error band of $\pm .3462$ fringes given by equation (21).

TABLE IV. Data for Error Analysis

		Figure 7	Figure 8	Figure 9
$\frac{\partial m}{\partial L}$ (fringes/in)		.484	.561	.929
dL (in)		.40	.48	.16
$\frac{\partial m}{\partial T_w}$ (fringes/°R)		.224	.228	.223
dT_w (°R)		.633	.633	.933
$\frac{\partial m}{\partial T_\infty}$ (fringe/°R)		-.203	-.202	-.182
dT_∞ (°R)		.333	.333	.333
dm (fringes)		.2687	.3462	.2967
$\frac{\partial T_{m+i}}{\partial L}$ (°R/in)	$(T_i=T_\infty)$	-2.23	-2.56	-4.10
	$(T_i=T_w)$	-2.45	-2.85	-4.89
$\frac{\partial T_{m+i}}{\partial T_i}$	$(T_i=T_\infty)$	.100	.116	.184
	$(T_i=T_w)$	.105	.122	.201
$\frac{\partial T_{m+i}}{\partial m}$ (°R/fringe)	$(T_i=T_\infty)$	4.45	4.39	4.47
	$(T_i=T_w)$	4.90	4.90	5.33
dT_{m+i} (°R)	$(T_i=T_\infty)$	.670	.663	1.068
	$(T_i=T_w)$	1.039	1.178	1.557

An analysis of the systematic error in temperature data is also necessary to support the temperature profile results. From equation (14b), the temperature can be expressed as a function of four variables,

$$T_{m+i} = T(L,T_i,m,P) \tag{23}$$

with the deviation due to pressure again considered to be negligible. Hence the systematic error can be expressed as

$$dT_{m+i} = \frac{\partial T_{m+i}}{\partial L} dL + \frac{\partial T_{m+i}}{\partial T_i} dT_i + \frac{\partial T_{m+i}}{\partial m} dm. \tag{24}$$

With the values for the partial derivatives evaluated from equation (14b) in a manner similar to that used in the evaluation of fringe error, an estimate of temperature deviation can be calculated. This deviation was computed assuming the initial temperature was the ambient air temperature, then assuming T_i was the wall temperature. The results are included in Table IV.

The small error band for both the fringe and temperature results further support the validity of the Gladstone-Dale optical theory to interferometric holography of temperature fields in a perfect gas.

II. THERMOCOUPLE CONSTRUCTION AND CALIBRATION

As was noted in the results, thermocouple data did not readily agree with the mathematical model or interferogram data. The major reason for this disagreement was due to the physical parameters of the thermocouple.

The thermocouples used in the experiment were constructed of copper and constantan. Both wires were of one foot length, .01 inches in diameter and teflon insulated. This insulation brought the diameter to a thickness of 3 mils. The two wires were welded together. The bead formed by the welding was approximately .026 inches in diameter. It is likely, due to the bead size, that the greatest error occurred. In some interferograms made, the bead was observed to overlap several fringes. This means the bead was located in an area of high temperature variation. It is likely that the temperature indicated was merely an average value.

The calibration of the thermocouples used was conducted against a Hewlett-Packard quartz thermometer Model 2801A. The quartz thermocouple is listed to have an accuracy of $\pm$ .02°C. Figure 21 is a calibration curve constructed from data obtained in this comparison. The value for the estimated error in thermocouple data was computed from this calibration curve.

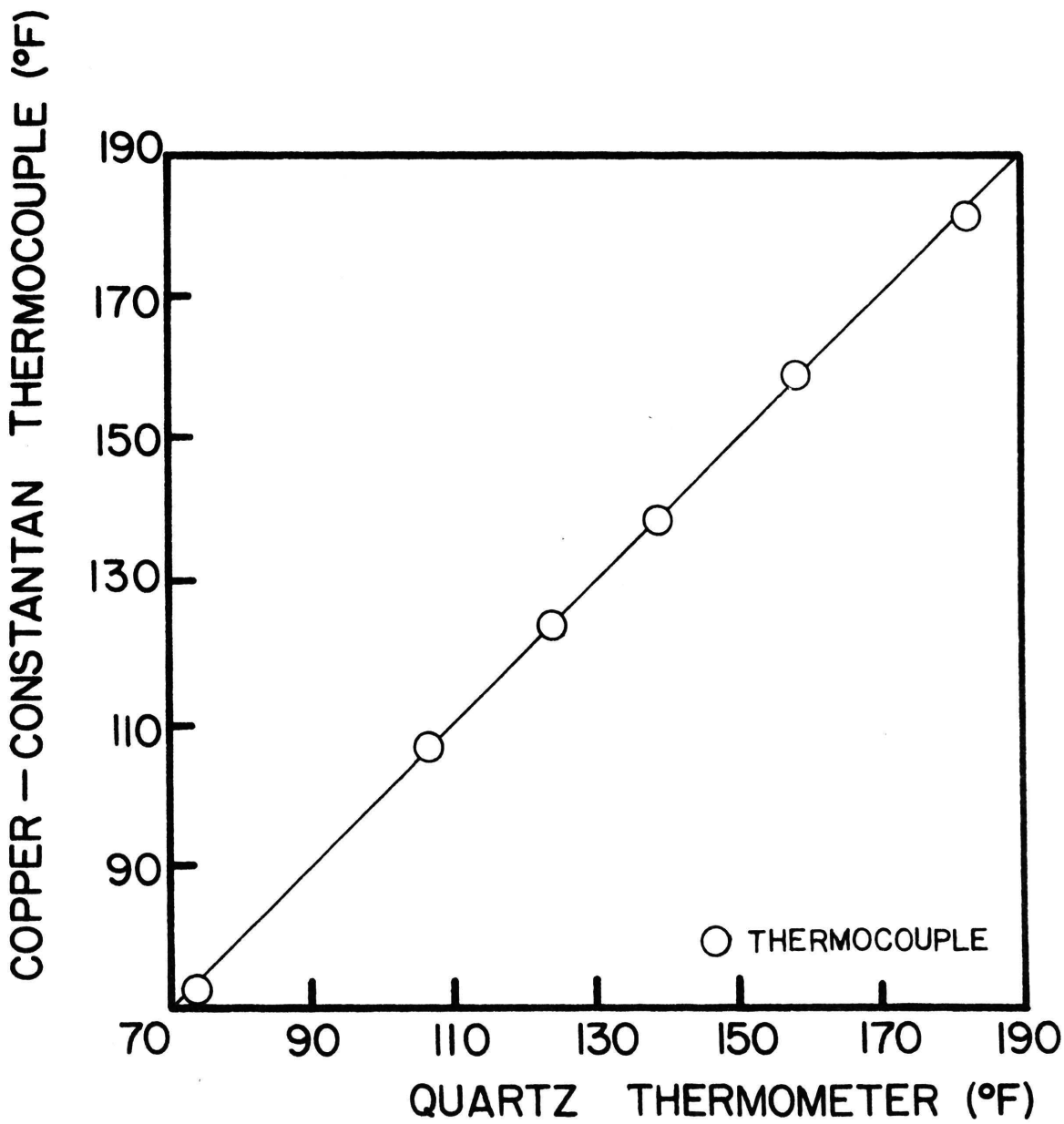

FIG. 21 THERMOCOUPLE CALIBRATION CURVE